

# A library of 0.5 to 2.5 $\mu\text{m}$ spectra of luminous cool stars

A. Lançon<sup>1</sup> and P.R. Wood<sup>2</sup>

<sup>1</sup> Observatoire de Strasbourg (UMR 7550), 11 rue de l'Université, F-67000 Strasbourg, France  
e-mail: lancon@astro.u-strasbg.fr

<sup>2</sup> Research School of Astronomy and Astrophysics, Australian National University, Private Bag, Weston Creek PO, ACT 2611, Australia  
e-mail: wood@mso.anu.edu.au

Received February 14; accepted July 7, 2000

**Abstract.** We present a library of 0.5 – 2.5  $\mu\text{m}$  digital spectra of cool, mostly variable, giant and supergiant stars which should be useful for spectral synthesis applications, as well as for comparison with theoretical model atmosphere calculations. The library includes carbon stars, Galactic Bulge and Magellanic Cloud stars, and OH/IR stars.

The stars observed cover a range of metallicities and masses. Most variable objects were observed several times, at different phases of their pulsation cycle. We discuss the effects of various fundamental parameters and of variability on the spectra. Based on period-luminosity relations and stellar evolutionary tracks, we tentatively assign initial masses to each object.

**Key words:** catalogs — stars: AGB — stars: individual: CL Car — stars: individual: R Lep — stars: variables: general — infrared: stars

## 1. Introduction

This paper presents a library of over hundred 0.5 – 2.5  $\mu\text{m}$  digital spectra of cool, mostly variable, giant and supergiant stars. The data set includes multiple observations of individual variable stars. The wavelength range covered contains most of the flux emitted by the sample stars. The spectral resolution in the near-IR is sufficient to identify molecular band substructures and the strongest individual metal lines. The data clearly have many applications in the field of purely stellar physics, but in the context of increasingly detailed studies of external galaxies the importance of this library for extragalactic work has to be highlighted.

*Send offprint requests to:* A. Lançon

One main aim of this paper is to provide a useful library of spectra of variable AGB stars for stellar population synthesis. AGB stars are the dominant contributors to the near-infrared light of an intermediate-age stellar population and a number of studies have been made of the contribution of AGB stars to broadband colours of stellar populations (Charlot & Bruzual 1991; Bressan et al. 1994; Maraston 1998; Lançon 1999; Lançon et al. 1999). The importance of the AGB stars to the near infrared light output of a stellar population is clearly demonstrated by the sudden jump in the  $V - K$  colour from  $\sim 1$  to  $\sim 3$  for a stellar population as it ages to the point where AGB stars form (Girardi & Bertelli 1998). Furthermore, at  $K$ , the thermally pulsing AGB (TPAGB) stars alone may contribute up to  $\sim 80\%$  of the population light, with the early AGB and other stars contributing the rest. Observations showing that all TPAGB stars are variable have recently become very convincing (Eyer & Grenon 1997; Wood et al. 1999). Thus the stellar spectra of intermediate-age populations should be dominated at  $K$  by *variable* AGB stars. Of course, the contribution of AGB stars to the integrated spectrum of a stellar population decreases with decreasing wavelength so that by  $R$  the contribution of AGB stars is small.

Among variable AGB stars, those with periods below 500 days provide the most significant contributions to the bolometric and to the near-IR luminosity of a stellar population. Indeed, stars with longer periods have very low effective temperatures and are usually reddened by circumstellar dust, two effects that combine to reduce even the near-IR contribution (Bressan et al. 1998, see also Girardi & Bertelli 1998). The sample of variable stars we have chosen therefore mostly contains optically visible stars with periods no longer than a few 100 days, although a small number of OH/IR stars have also been included. Carbon stars were also observed, because they represent a large fraction of the AGB stars in metal deficient environments (e.g. the Magellanic Clouds) and in various plausible

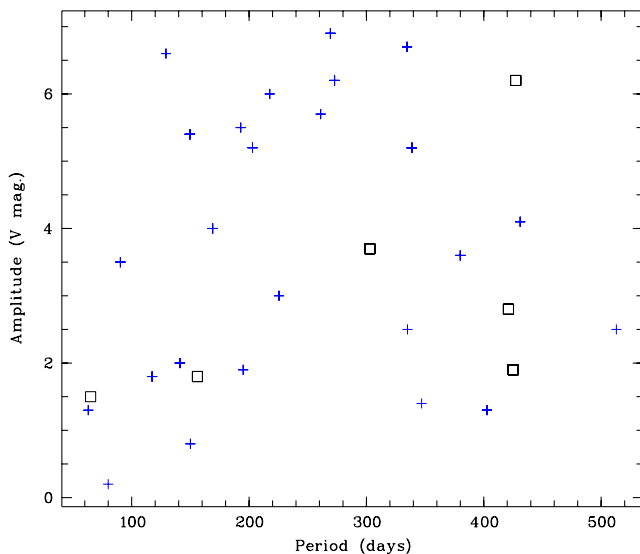


**Fig. 1.** Period - amplitude distribution of the variable stars in the sample. Crosses and squares, respectively, represent oxygen and carbon rich objects. Stars with unknown periods or amplitudes (among which are our coolest objects) have not been plotted. The majority of the programme stars are miras and semi-regular variables of the solar neighbourhood. In addition, a small sample of Magellanic Cloud stars and Galactic Bulge stars were included. The Magellanic Cloud LPVs were selected from the brighter O-rich sources of the sample of Wood et al. (1983). The Bulge objects were selected among the Sgr I and NGC 6522 field LPVs of Wood & Bessell (1983), with the additional criterion that they be red ( $J - K > 2$ ) because such extreme colours were interpreted by the authors as the result of high metallicity. Finally, for comparison purposes a few giants and red supergiants with insignificant variations were included

synthetic populations (Marigo et al. 1999; Mouhcine et al., in preparation). Overall, an effort was made to sample the three-dimensional parameter space of spectral type, period and amplitude (Fig. 1), based on the information provided in the General Catalogue of Variable Stars (GCVS, Kholopov et al. 1988).

Stellar and extragalactic studies are not disconnected. Models designed to predict synthetic spectra for pulsating red giants are progressing rapidly (Bessell et al. 1989b; Hofmann et al. 1998; Höfner et al. 1998; Alvarez & Plez 1998; Loidl et al. 1999; Hauschildt et al. 1999), but are still in their infancy. They are needed as a link between the empirical spectra and the theoretical evolutionary tracks along the AGB. The latter provide the evolution of the global properties (luminosity, effective temperature, surface abundances) of the static so-called parent stars of Mira variables but it is poorly known, for instance, how much lower the effective temperatures become once pulsation has been allowed for. The concept of effective temperature itself becomes unclear due to the extreme extension of the atmospheres of Mira stars, and the relation between

photometric/spectroscopic properties and the theoretical effective temperature remains to be understood and calibrated. Comparison of the model predictions with the data in this paper will assess the current reliability of the models. Two features of the present library make it particularly valuable for this comparison: the broad wavelength coverage, which makes the simultaneous study of the global energy distribution and the spectral features possible, and the inclusion of sequences of observations of individual stars at various phases over one or a few pulsation cycles.

The data are described in Sect. 2. Section 3 discusses a selection of properties of the sample of spectra, including effects of variability and of metallicity. Stars of particular interest, deserving further study, are identified in that section and in the Appendix. In Sect. 4, we discuss the evolutionary status of the observed objects, a piece of information relevant both to population synthesis applications and to the comparison of the spectra with stellar model predictions.

## 2. Observations and data reduction

### 2.1. Near-IR observations

The near-IR spectra were obtained with the Australian National University 2.3 m Telescope at Siding Spring Observatory, using the cross-dispersed grism mode of the Cryogenic Array Spectrometer and Imager CASPIR. This camera operates at 70 K with a Santa Barbara Research Center CRC463 256×256 InSb array maintained at 32 K (complete information is given in the CASPIR manual, McGregor 1994).

For each of the *IJ*, *JH* and *HK* grisms, five orders are imaged onto the CASPIR array. As can be seen from Table 1, there is a significant overlap between orders and grisms. The spectra were acquired through the  $1'' \times 15''$  slit, providing a resolving power  $\lambda/\delta\lambda \simeq 1100$ . In photometric weather conditions, an additional low resolution *HK* band spectrum was taken through a  $10''$  wide slit and used to recover the absolute flux calibration.

For optimal dark current and sky subtraction, “ABBA” observing sequences were followed. The star was shifted + or  $-4''$  along the  $1''$  slit, or moved in and out of the  $10''$  slit between A and B exposures. An ABBA sequence consisted of at least four 30 s exposures, each of which consisted of 2 to 100 individual readouts of the array depending on the brightness of the object. For the removal of telluric absorption features and the flux calibration, both O, B stars and late F or early G dwarf stars with known near-IR magnitudes were observed (typically one reference for every 4 or 5 programme observations).

**Table 1.** Orders of the CASPIR gratings

grism	order	$\lambda_{\min}$ (Å)	$\lambda_{\max}$ (Å)
<i>IJ</i>	16	9700	10850
	15	10 290	11 490
	14	10 950	12 220
	13	11 700	13 050
	12	12 570	14 010
<i>JH</i>	17	12 470	13 890
	16	13 150	14 640
	15	13 920	15 480
	14	14 780	16 420
<i>HK</i>	13	15 770	17 490
	13	16 100	17 980
	12	17 320	19 320
	11	18 740	20 880
	10	20 400	22 710
	9	22 420	24 900

## 2.2. Near-IR data reduction

The data was reduced with IRAF software, using the CASPIR reduction package (P. McGregor, CASPIR manual) and extensions thereof (A.L.). After subtraction of a median bias frame, a quadratic correction for the non-linearity of the response was applied (typically less than 1%) and ABBA sequences were combined. An internal incandescent lamp provided the light-on-light-off flatfields, which were then divided into the data frames. The traces of stars at two positions in the slit and both xenon and argon arcs were used to derive the geometrical transformation into straightened, wavelength calibrated images of the individual grism orders, from which the spectra were extracted and co-added. No additional sky subtraction was usually required. The wavelength calibration is accurate to better than 2 Å.

It is a well known problem that no spectrophotometric standards, in the sense familiar to optical observers, exist for near-IR flux calibration. The determination of the telescope, instrument and atmosphere transmission functions relies on the comparison of the observed reference star spectra with model atmosphere calculations. Ideally, objects with intrinsically featureless spectra are required for the removal of telluric features, and objects with known energy distributions for the relative spectrophotometric calibration. With 10 m class telescopes, increased sensitivities will make it possible to use featureless white dwarf spectra for the first purpose. Some currently feasible approaches based on A, F and early G type stars have been described by Hanson et al. (1996) and Maiolino et al. (1996). As far as telluric absorption is concerned the method followed here was similar, but extended to a much broader wavelength range. This spectral extent prohibits the use of blackbody curves to mimic the intrinsic energy distributions of the reference stars.

O, B and A stars have few intrinsic lines apart from the hydrogen (and sometimes helium) series and are easier to use than solar type references over most of the spectral range. However, their lines are often deep and broad, with complex profiles that vary from one line to the other, and the Brackett hydrogen lines are blended around 1.6  $\mu\text{m}$  at our resolution. Removing them is not as easy as one could have hoped. In addition, early type stars are not evenly distributed on the sky and they are often found in dusty environments. Their use as relative flux standards requires the knowledge of the foreground extinction as well as their intrinsic energy distribution. F and early G dwarf stars display weaker but more numerous absorption features. Their energy distributions depart significantly from those of blackbodies, but at temperatures around 6000 K the Kurucz atlas (1993) provides reliable representations (as discussed in Lejeune et al. 1997; Castelli et al. 1997; Bessell et al. 1998). Our calibration procedure was based on both early and intermediate type reference stars and can be outlined as follows.

To select the most adequate model spectrum from the library of Kurucz (1993), the literature was searched reference star by reference star for individual estimates of the effective temperature, the surface gravity, the metallicity and the extinction on the line of sight (cf. Table 2). The corresponding Kurucz spectra were reddened when required, using the reddening law of Cardelli et al. (1989). All the raw extracted reference star spectra of a night were compared to each other and to theoretical spectra order by order. In this procedure, it was found extremely useful to be able to overlay early and intermediate type spectra in order to identify and distinguish between the strong stellar lines and the numerous telluric lines (cf. Fig. 2). The division of the models into the data, and interpolation across regions affected by strong stellar lines, then provided the combined throughput of the instrument and the atmosphere at the time of each reference observation.

Finally, each programme star was corrected with each of these transmission functions, the five orders of each grism were merged (there was no need for any additional scaling or shifting) and the results for each transmission function were compared. Depending on the stability of the weather conditions and of the instrument, the most important criterion for the selection of the final spectrum was either the similarity of the airmass or the closeness in time with the reference observation. The telluric CO<sub>2</sub> features around 2.00 and 2.05  $\mu\text{m}$  are easy to identify and correlate tightly with airmass, whereas the broad H<sub>2</sub>O absorption bands can vary independently of the airmass on timescales sometimes shorter than an hour. In about 20% of the cases, a second order correction of either the CO or the H<sub>2</sub>O bands was performed, using ratios of transmission functions normalised to 1 in the atmospheric windows. However, since the recorded signal virtually drops to zero in the deepest water bands (especially in Summer),

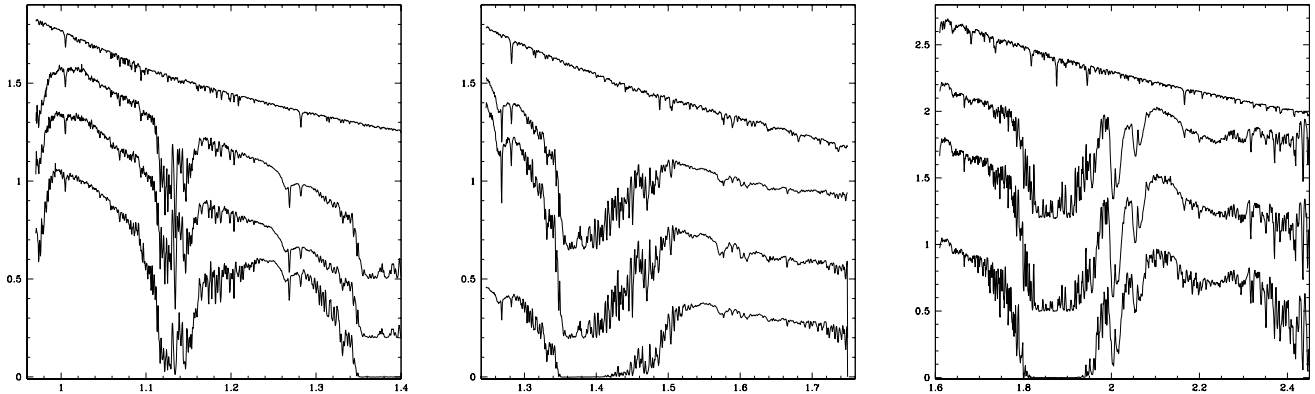


**Fig. 2.** Raw *IJ*, *JH* and *HK* spectra of the G0V star BS 77 taken (from bottom to top) on one of the worst moist Summer nights (airmass 1.3), on a normal Summer night (1.6) and on a normal Winter night (1.2). The solar spectrum (Castelli 1996, private communication) is shown for comparison; its slope has been adjusted for display purposes. All spectra have been rescaled to a similar mean flux and then spaced. Note that changes in the slopes of the raw spectra are partly due to changes in the instrumental response between runs

the energy distribution could only rarely be completely recovered.

A total of 28 stars were used as references over the course of the 21 near-IR observing nights, forming a network that allowed us to cross-check the model selections between nights. The reference stars and the model adopted for each of them are listed in Table 2.

When  $10''$  slit *HK* spectra were available, they were corrected in a similar manner but an absolute flux calibration was also achieved, based on the known *K* band magnitudes of the reference stars. The high resolution spectra were then scaled to the level of the corresponding flux-calibrated low resolution ones.

### 2.3. Optical spectra

Low resolution optical spectra were acquired quasi-simultaneously with the infrared spectra using the Reynolds Spectrograph on the 1.88 m Telescope at Mount Stromlo Observatory. The spectrograph was used with a 150 l/mm grating in first order (2 deg. Blaze angle, giving a dispersion of  $9.7 \text{ \AA}/\text{pixel}$ ), an order selecting filter with a cut-off at  $5000 \text{ \AA}$  (GG 495, but GG 550 in June 95) and a 4 arcsec slit. The spectral resolution was usually seeing-limited, giving a FWHM resolution between 30 and  $40 \text{ \AA}$  instead of the slit-limited  $50 \text{ \AA}$ . Standard IRAF routines were used for the reduction of the data. The transformation to wavelengths coordinates was very close to linear. An additional zero point shift was required subsequently, correcting for the position of the star in the slit and instrumental instabilities: the wavelength of  $H\alpha$  was forced to  $6565 \text{ \AA}$  when present, and a cross-correlation in spectral regions with strong telluric features was used to determine the shift for the remaining spectra. The distribution

of residual wavelength errors has a standard deviation of about  $3 \text{ \AA}$ .

The flux calibration and removal of atmospheric features were based on a selection of spectrophotometric standards whose intrinsic spectra (themselves corrected for telluric absorption) were provided by M. Bessell.

### 2.4. Quality of the resulting spectra

The resulting optical data set consists of about 200 spectra with a typical signal-to-noise ratio per resolved element of 50, except in regions of strong telluric absorption ( $7605 \text{ \AA}$ ,  $9000 - 9800 \text{ \AA}$ ). In the comparison of two optical spectra, changes in the (seeing limited) spectral resolution and calibration are the origin of most of the noise. The energy distribution between  $5500 \text{ \AA}$  and  $9000 \text{ \AA}$  is recovered to within 5% ( $1 \sigma$ ), but the uncertainties rise to 10% below  $5300 \text{ \AA}$  and around  $9500 \text{ \AA}$ .  $V' - I$  (where  $V'$  is a  $V$  filter cut off below  $5000 \text{ \AA}$ ) can be measured to  $\pm 0.15$  magnitudes and individual molecular features can be measured to within a few percent.

In the near-IR, there are 140  $0.97 - 2.49 \mu\text{m}$  spectra of 55 programme stars (Table 3). The comparison between calibrations with various standards and the comparison of individual stars between nights indicate a typical signal-to-noise ratio per resolved element of 50 in atmospheric windows. It drops in the areas of strong telluric  $\text{H}_2\text{O}$  or  $\text{CO}_2$  absorption shown in Fig. 2. On scales of  $\sim 50 \text{ \AA}$ , bumps or dips at the 5% level sometimes remain as the residuals of an imperfect removal of internal reflections in the instrument (they are most obvious around  $1.25 \mu\text{m}$ ; however in most cases the features seen in this range are real).

The uncertainties on the energy distribution (colours) result from the combined effects of instrumental changes,

**Table 2.** Reference stars for near-IR spectroscopy

	Star	Type	Nights (JD-2400000)	Model
1	BS 33	F7V	17.6.95 (49886), 7.7.96 (50272)	t6250m00, $A_v = 0.11$
2	BS 77	F9V	9.12.95 (50061), 30.1.96 (50113), 7.7.96 (50272)	t6000m00, $A_v = 0.$
3	BS 674	B8IV-V	3.3.96 (50146)	t13000m00, $A_v = 0.$
4	BS 818	F6V	20.11.97 (50773)	t6500m00, $A_v = 0.03$
5	BS 1006	G2V	8.12.95 (50060), 7.7.96 (50272)	t5750m10, $A_v = 0.$
6	BS 1291	F2V	8.12.95 (50060)	t6750m00, $A_v = 0.05$
7	BS 1502	F2V	3.3.96 (50146), 7.7.96 (50272)	t7000m00, $A_v = 0.$
8	BS 2015	A7V	8.12.95 (50060)	t7500m00, $A_v = 0.13$
9	BS 2451	B8III	29.1.96 (50112), 20.11.97 (50773)	t11000m00, $A_v = 0.04$
10	BS 3034	B0Ve	19.2.95 (49768)	t29000m00, $A_v = 0.74$ , hot gas
11	BS 3138	G0V	11.4.95 (49819), 8.12.95 (50060), 29.1.96 (50112)	t6000m10, $A_v = 0.$
12	BS 3578	F7V	12.4.95 (49820), 8.12.95 (50060), 3.3.96 (50146) 26.5.96 (50230), 27.5.96 (50231)	t6000m10, $A_v = 0.$
13	BS 4102	F2IV	3.3.96 (50146), 30.3.96 (50173), 25.5.96 (50229) 26.5.96 (50230), 8.7.96 (50273)	t6750m00, $A_v = 0.$
14	BS 4133	B1Ib	16.2.95 (49765)	t20000m00, $A_v = 0.21$
15	BS 4600	F6V	11.4.95 (49819), 25.5.96 (50229), 8.7.96 (50273)	t6500m00, $A_v = 0.09$
16	BS 4638	B3V	16.2.95 (49765), 29.1.96 (50112), 30.1.96 (50113)	t18000m00, $A_v = 0.15$
17	BS 4743	B2V	16.2.95 (49765), 8.7.96 (50273)	t20000m00, $A_v = 0.12$
18	BS 4757	B9.5V	25.5.96 (50229)	t10000m00, $A_v = 0.13$
19	BS 4773	B5V	18.6.96 (50253), 31.3.96 (50174), 26.5.96 (50230) 27.5.96 (50231)	t15000m00, $A_v = 0.05$
20	BS 4903	B1V	16.2.95 (49765)	t5750m00, $A_v = 0.$
21	BS 4989	F7IV	3.3.96 (50146), 31.3.96 (50174)	t6000m05, $A_v = 0.$
22	BS 5993	B1V	17.6.95 (50252), 26.5.96 (50230), 27.5.96 (50231) 6.7.96 (50271)	t25000m00, $A_v = 0.75$
23	BS 6310	F3V	2.3.96 (50145), 6.7.96 (50271), 8.7.96 (50273)	t6750m00, $A_v = 0.$
24	BS 6314	F6V	11.4.96 (50185)	t6250m00, $A_v = 0.$
25	BS 6496	F7V	18.6.95 (50253), 3.3.96 (50146)	t6250m00, $A_v = 0.$
26	BS 7213	F7V	11.4.96 (50185)	t7000m00, $A_v = 0.$
27	BS 7446	B1III	26.5.96 (50230), 27.5.96 (50231)	t25000m00, $A_v = 0.88$
28	BS 7875	F8V	17.6.95 (50252), 7.7.96 (50272)	t6000m00, $A_v = 0.03$

*Notes:* Model descriptions are given as tXXXXmZZ, where XXXX is the effective temperature ( $T_{\text{eff}}$ ), and ZZ indicates the metallicity ( $-\log(Z/Z_{\odot})$ ). Theoretical spectra: Kurucz (1993),  $\log(g) = 4.5$  (using lower surface gravities for O, B stars has no significant effect on the near-IR colours).  $T_{\text{eff}}$  and metallicities were chosen according to the literature when available. Otherwise  $Z_{\odot}$  was adopted and an approximate  $T_{\text{eff}}$  was derived from the spectral type; agreement with the known near-IR colours of the stars was given priority over compliance with a unique  $T_{\text{eff}}$ -spectral type relation. Except for BS 7446 (Theodossiou 1985), non-zero optical extinction values are from Neckel et al. (1980).

The model adopted for BS 3034 combines the photosphere model with a gas emission model (Dachs & Wamsteker 1982). Both contributions are reddened and contribute equally to the emission at  $2.45 \mu\text{m}$  (in order that the resulting model colours agree with the observed ones to within 0.03 mag).

the focusing and positioning of the stellar image on the slit and the choice of a model for the intrinsic spectrum of the reference stars. Figure 3 illustrates the estimated quality of the relative flux calibration in the near-IR, again based on the comparison between reference star spectra taken at different times. After a systematic reduction of all data, we estimate that at least 85% of the spectra have errors smaller than indicated on the plot while the errors for the 15% most uncertain spectra don't exceed the values of Fig. 3 by more than 50%.

The 108 pairs of matching optical and near-IR spectra may be merged by scaling the spectra to the same mean in the most reliable part of the region of overlap (the range

9760 – 9870 Å). As mentioned above, this wavelength range suffers from relatively high uncertainties in the optical spectra, leading to an uncertainty of 0.15 mag in  $I - J$  and in all other colours combining optical and near-IR fluxes. Quadratic summing of the uncertainties across the optical and near-IR ranges, combined with the connection uncertainty at 9760 – 9870 Å, results in a total uncertainty of  $\sim 0.3$  mag in  $V' - K$  (note that  $V' - K \sim 3.6 - 7.3$  for M 0–M 6 stars, respectively).

The potential user of the final data should not hesitate to contact the authors (A.L.) for additional information, especially if his/her aim is to study the detailed variations

**Table 3.** Programme stars: main properties, number of spectra

Name	1950	vartype	$V$ (at min)	$\delta V$	$P$ (days)	epoch (at max)	Sp.type	Nobs (VK/VI/IK)	Figure
(1)	(2)	(3)	(4)	(5)	(6)	(7)	(8)	(9)	(10)
<i>Oxygen rich variables</i>									
WX Psc	01 03 48 + 12 19 51	M	>12.5	>2.5	645 <sup>b</sup>	—	M9III (OH/IR)	0/0/1	B24
RS Hor	02 34 36 – 62 48 06	M	15.0	5.2	202.9	30100	M3e	3/3/3	B13
X Men	03 33 40 – 76 36 57	M	15.0	3.6	380.0	28720	M3e	4/4/4	B19
R Cnc	08 13 48 + 11 52 52	M	11.8	5.6	361.7	38093	M7IIIe	0/1/0	
R Cha	08 22 56 – 76 11 36	M	14.2	6.7	334.6	42006	M4e-M7e	4/5/5	B10
SY Vel	09 10 35 – 43 34 16	SRb	10.2	1.3	63.0	—	M5/6III	2/3/2	B6
UZ Hya	09 14 15 – 04 23 48	M	14.5	5.7	261.0	42527	M4e	2/2/2	B16
CM Car	09 46 44 – 67 12 48	M	14.0	2.5	335.0	—	M2e	1/3/1	B11
S Car	10 07 46 – 61 18 14	M	9.9	5.4	149.5	42112	K5e-M6e	6/8/8	B7
KV Car	11 01 08 – 66 51 26	SRb	10.6	0.8	150.0	—	M4III	2/6/2	B4
RZ Car	10 34 13 – 70 27 29	M	15.0	6.2	272.8	39586	M4e-M8e	5/7/7	B8
RS Hya	10 48 57 – 28 21 43	M	14.4	5.2	338.6	39169	M6e	5/7/7	B15
U Crt	11 10 15 – 07 01 30	M	13.5	4.0	169.0	28269	M0e	2/5/3	B12
BD Hya	11 13 42 – 29 54 23	SRa	12.2	1.8	117.4	27900	M0e-M2	3/7/4	B14
SW Hya	13 00 38 – 28 50 14	M	13.0	3.2	218.8	29302	M2e	0/1/0	
V603 Cen	13 02 04 – 35 19 22	M	13.4	2.3	253.0	38898	K0	0/1/0	
T Cen	13 38 53 – 33 20 42	SRa	9.0	3.5	90.4	43242	K0e-M4e	4/5/4	B9
ET Vir	14 08 06 – 16 04 00	SRb	5.0	0.2	80.0	40697	M2III	1/2/1	B1
AFGL 1686	14 08 39 – 07 30 42	M	>12.5	>2.5 <sup>b</sup>	700: <sup>b</sup>	—	M8III (OH/IR)	0/0/2.5 <sup>a</sup>	B24
AO Cen	14 57 34 – 42 17 52	M	12.5	1.9	189.0	13627	M2e	0/2/0	
S Lib	15 18 31 – 20 12 33	M	13.0	5.5	192.9	41883	M1.0e-M6.0e	2/3/2	B17
RS Lib	15 21 24 – 22 44 04	M	13.0	6.0	217.6	42154	M7e-8.5e	2/3/2	B18
R Cir	15 23 57 – 57 33 10	SRb	12.1	1.9	222.0	—	M4/6III	0/1/0	
SV Lib	15 30 20 – 27 01 00	M	11.5	1.3	402.7	33852	M8e	3/5/3	B5
Z Lib	15 43 36 – 20 58 23	M	14.0	3.6	298.6	27689	M3e	0/1/0	
R Ser	15 48 23 + 15 17 03	M	14.4	8.7	356.7	37010	M7IIIe	0/1/0	
DX Ser	16 06 00 – 01 24 23	SRa	12.4	2.0	360.0	33880	M5-M8	0/1/0	
WW Sco	16 24 11 – 31 11 33	M	14.7	4.1	431.0	19944	M6e-M9	2/3/3	B22
RY Cra	18 18 18 – 44 55 30	M	14.0	1.9	195.0	28845	M4e	1/1/2	B11
SV Tel	18 52 28 – 49 32 03	M	13.2	3.0	225.5	30045	M4e-M6e	1/1/2	B23
Z Aql	20 12 31 – 06 18 17	M	14.8	6.6	129.2	41938	M3e	0/0/2	B23
U Equ	20 54 45 + 02 47 10	M?	>15.5	>1	—	—	OH/IR	0/0/0.5 <sup>a</sup>	B24
R Phe	23 53 52 – 50 03 55	M	14.4	6.9	269.3	39486	M2IIe-M4IIIe	4/5/5	B20
S Phe	23 56 30 – 56 51 14	SRb	10.6	2.0	141.0	—	M3e-M6IIIe	4/5/5	B21
<i>Carbon rich variables</i>									
T Cae	04 45 32 – 36 17 50	SR	10.8	1.8	156	27840	C6,4(N4)	3/3/3	B27
R Lep	04 57 20 – 14 52 48	M	11.7	6.2	427.1	42506	C7,6e(N6e)	3/3/5	B31
RU Pup	08 05 20 – 22 46 00	SRb	12.2	1.9	425	—	C5,4(N3)	5/5/7	B30
Y Hya	09 48 45 – 22 46 57	SRb	12.0 <sup>c</sup>	3.7 <sup>c</sup>	302.8	—	C5,4(N3P)	6/7/7	B29
BH Cru	12 13 37 – 56 00 29	M	10.0	2.8	520 <sup>d</sup>	40858	SC4.5/8e	3/5/3	B28
S Cen	12 21 52 – 49 09 47	SR	10.7	1.5	65	43242	C	1/2/1	B27
V Oph	16 23 56 – 12 18 54	M	11.6	4.3	297.2	45071	C5,2/7,4e(N3e)	0/1/0	

*Notes to Table 3:*

The columns are: Name (Col. 1), right ascension and declination (Col. 2), the variability type (Col. 3),  $V$  magnitude at minimum light (Col. 4),  $V$  amplitude (Col. 5), period (Col. 6), phase 0 epoch (visual maximum) expressed as JD–2400000 (Col. 7), and spectral type (Col. 8). All these quantities were taken from the GCVS (Kholopov et al. 1988). Column 9 gives the number of merged (VK), optical (VI) and infrared (IK) spectra available.

(a) A fractional value indicates an incomplete infrared spectrum. (b) Jones et al. (1990).

(c) AAVSO/AFOEV data suggest a significantly smaller amplitude, but non-detections need to be assessed for a quantitative statement (AFOEV 1999, Mattei 1999). (d) Period has increased (Bedding et al. 2000), GCVS period = 421 d.

**Table 4.** LMC/SMC stars (Fig. B26)

Star	1950	Period	$K$	$J - K$	Nobs (vK/vI/IK)
HV 2255 (LMC)	04 58 08 – 70 13 15	830	7.4	1.2	1/1/1
N371 R20 (SMC)	00 59 02 – 72 26 47	580	8.2	1.0	1/1/1
HV 2446 (LMC)	05 20 07 – 67 23 08	602	9.2	1.2	1/1/1
HV 2360 (LMC)	05 12 49 – 67 23 08	790	7.7	1.1	1/1/1

**Table 5.** Bulge stars (Fig. B25)

Number	1950	Period	$K$	$J - K$	Nobs
<i>NGC 6522 field:</i>					
205	17 59 06 – 29 59 17	470:	6.31	2.27	0/0/1
426	17 59 28 – 30 05 26	465	6.57	2.03	1/1/1
435	17 59 17 – 30 06 47	465	6.59	1.97	1/1/1
<i>SGR I field:</i>					
4	17 55 44 – 28 50 32	450:	5.89	1.55	1/2/3
117	17 57 35 – 29 11 00	360	6.91	1.84	0/1/1
5	17 55 12 – 28 49 14	450:	6.47	1.78	0/1/0
21	17 55 29 – 29 01 13	355	7.96	1.64	1/2/2
11	17 56 46 – 28 53 23	750 <sup>a</sup>	6.25	1.81	1/2/2
55	17 56 18 – 29 03 11	330	7.37	1.8	0/1/1

Notes to Tables 4 and 5:

The Bulge and Magellanic Cloud data have a lower signal-to-noise ratio than the local stars.

(a) Lloyd Evans (1976) finds  $P = 405$  days.

**Table 6.** Red giant and supergiant stars

Name	2000	Type	Nobs (vK/vI/IK)	Figure	Comments
<i>Giants:</i>					
BS 4104	10 27 09 – 31 04 04	K4III	0/1/0		
BS 4432	11 30 18 – 03 00 12	K4.5III	1/2/1	B1	
BS 5797	15 38 03 – 42 34 03	M0III	0/1/0		
BS 4371	11 14 43 + 02 17 08	M0III	1/2/1	B1	
BS 2608	06 56 16 – 48 43 16	M1III	0/1/0		
BS 4517	11 45 51 + 06 31 46	M1III	0/1/0		
BS 3923	09 54 53 – 19 00 46	M1III	1/2/1	B1	
BS 4463	11 35 13 – 47 22 22	M3III	0/2/0		
BS 4807	12 38 22 + 01 51 17	M3III	0/1/0		
BS 1695	05 07 34 – 63 23 59	M4III	0/1/0		
BS 5603	15 04 04 – 25 16 55	M4III	0/1/0		
BS 4532	11 48 45 – 26 45 24	M4III	0/1/0		
BS 4267	10 56 01 + 06 11 11	M5III	1/2/1	B1	$\delta V = 0.3$
<i>Supergiants:</i>					
HD 106873	12 17 46 – 63 36 58	M0I	1/1/1	B2	Lb, $\delta V = 1.5$
HD 98817	11 21 39 – 60 59 28	M1I	1/1/1	B2	
BS 3364	8 30 30 – 36 43 17	M2I	1/1/1	B2	
HD 101712	11 41 49 – 63 24 52	M2-3I	2/3/2	B2	
IRC –20427	18 05 35 – 21 13 39	M2I	0/0/1	B3	
HD 115283	13 17 25 – 61 35 02	M4I	1/1/1	B2	$\delta V = 0.6$
UY Sct	18 27 36 – 12 27 59	M4I	1/1/1	B3	SR, $\delta V = 1.5$
V774 Sgr	17 54 26 – 23 14 09	M4-5I	1/1/1	B3	Lb, $\delta V = 1.4$
EV Car	10 20 22 – 60 27 16	M4.5Ia	1/3/1	B3	SR, $\delta V = 1.4$ , $P = 347$
CL Car	10 54 00 – 61 05 31	M5Iab	1/1/1	B3	SRc, $\delta V = 2.50$ , $P = 513$

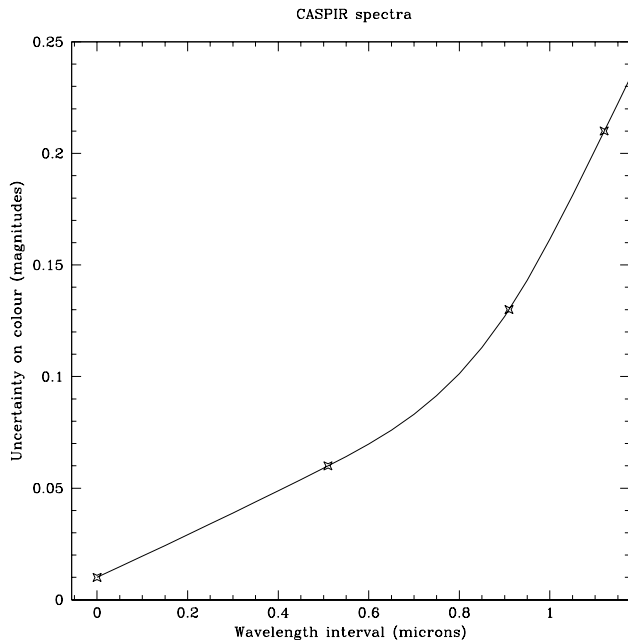


**Fig. 3.** Uncertainty on broad band colour indices measured on CASPIR spectra of this programme, as a function of the separation between the central wavelengths of the two passbands defining the colour (avoiding the regions of heavy telluric absorption). Estimates are based on non-variable reference stars observed several times, and on differences between spectra obtained with the different flux calibration standards of one night. The solid line is an interpolation through the uncertainty estimates obtained by comparing fluxes in filters centered at 1.04, 1.25 and 1.65  $\mu\text{m}$ , to the flux around 2.16  $\mu\text{m}$

of one particular object or one particular spectral feature (instead of studying statistical properties).

### 2.5. The final data

The reduced spectra are presented as a series of figures at the end of this paper. Merged optical/near-IR pairs are plotted when available, single near-IR spectra are plotted as next preference while single optical spectra are only shown in particular cases. The plotted spectra are normalised to a common mean flux per unit wavelength and then shifted for display purposes.

All spectra are also available in numerical form through CDS<sup>1</sup>. We provide the optical and near-IR spectra separately with names of the form *nameVI.Rdate* (ex. ScarVI.R1mar96) and *nameIK.Cdate* (ex. ScarIK.C3mar98), respectively, and, when applicable, the merged spectra of matching pairs with names of the form *nameVK.date* (ex. ScarVK.mar96). There are 182 VI spectra, 142 IK spectra and 108 VK spectra.

<sup>1</sup> Centre de Données Astrophysiques de Strasbourg, <http://cdsweb.u-strasbg.fr/CDS.html>, VizieR service.

Finally, a series of tables made available electronically contain, for each spectrum:

- the date of the observation;
- the reference star used for removal of telluric features and flux calibration (IK spectra only);
- the phase of the observation (when period and zero point available);
- a flag indicating whether or not absolute flux calibration has been achieved;
- an estimate of the stellar luminosity based on the period-K luminosity relation of Hughes & Wood (1990) and on the bolometric correction estimated from the spectrum itself (for merged VK spectra only).

### 3. Selected results

The data set provides an immense amount of information. Our purpose here is to draw attention to selected empirical facts that do, in our opinion, deserve further investigation either observationally or theoretically. We also identify individual stars of special interest.

The use of near-IR molecular indices for classification purposes is discussed by Alvarez et al. (2000). Ways to include the data in population synthesis calculations and first results are presented in Lançon (1999), Mouhcine & Lançon (1999 a,b, 2000) and Lançon et al. (1999). The construction of a practical library of suitably averaged empirical LPV spectra and a discussion of the appropriate temperature scale will be presented in more detail in a forthcoming paper (Mouhcine et al., in preparation). First comparisons of the empirical data with the O-rich LPV model spectra described in Bessell et al. (1991, 1996) and Hofmann et al. (1998), and with the carbon star models of the Vienna group (Loidl et al. 2000) have been made, and will be reported in detail elsewhere.

#### 3.1. Line and band identifications

The optical spectra of late-type O-rich stars are shaped by TiO and VO bands. Identifications are given in Phillips (1969), Turnshek et al. (1985), Brett (1989, 1990) and Valenti et al. (1998), and are shown in Fig. 4. The Ca II triplet (8498, 8542 and 8662 Å) is seen in stars of early M spectral type (Figs. B1, B2, and B9, but disappears when TiO absorption takes over for later types and in most LPV spectra of the present sample. Identifications for features between 1 and 1.3  $\mu\text{m}$  are given by Joyce et al. (1998). The H<sub>2</sub>O band around 1.15  $\mu\text{m}$  is easily confused with the CN band present in red supergiants, and is heavily blended with TiO and VO bands in the coolest LPVs. For easier comparison with the data of Joyce et al. (1998), Fig. 5 provides an enlargement of this region for a variety of cool stars, on the wavenumber scale adopted by these authors. At longer wavelengths, CO and H<sub>2</sub>O are



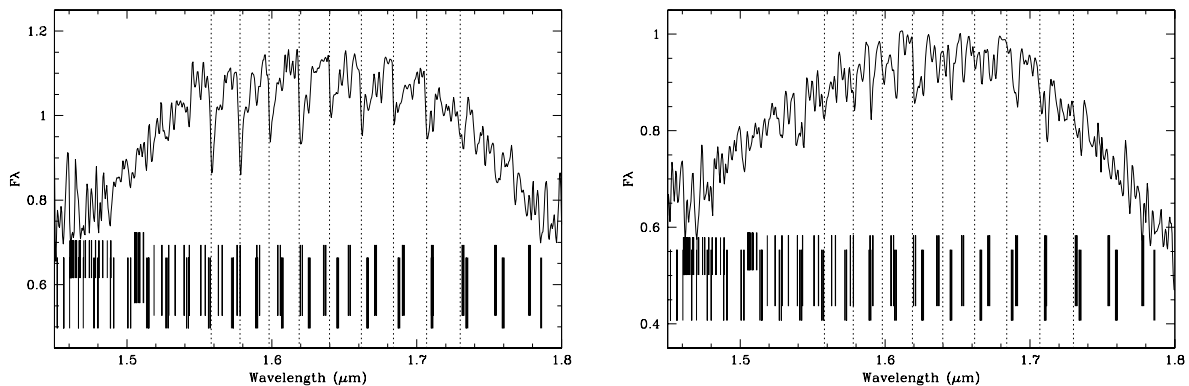


**Fig. 6.** Relative importance of CO and OH in the H window, in the Miras SV Lib (left) and S Car (right). The dotted lines identify the main  $^{12}\text{CO}$  bandheads. Vertical marks identify OH lines. Throughout the window, the 2–0 P series (lower long marks) and 3–1 P series (higher long marks) are seen; the 3–1 Q (1.51  $\mu\text{m}$ , short marks) and R series (1.46  $\mu\text{m}$ , short marks) are also shown. The curved shape of the spectra is due to  $\text{H}_2\text{O}$  absorption

The spectra of LPVs with small visual amplitudes ( $\leq 1.3$ ) are similar to those of static stars. They can be sorted into the giant or supergiant categories using the two-colour diagram shown in Fig. 7. The GCVS supergiant classification of the variables EV Car (SRb), CL Car (SRc), UY Sct (SR) and V774 Sgr (Lb) is confirmed. ET Vir (SRb,  $\delta V = 0.2$ ) obviously joins the giants (Fig. B1), and SY Vel (SRb,  $\delta V = 1.3$ , Fig. B6) shows very little difference with the M 5 giant BS 4267 (Fig. B1). KV Car (SRb,  $\delta V = 1.3$ ) significantly varied between our two observations; although they show relatively strong CO bands, this star’s spectra fit into the spectral sequence of giants.

Strong  $\text{H}_2\text{O}$  bands are found to be the characteristic feature of *variable* M stars. Inside subsamples of M type stars with similar optical spectra and global energy distributions, very different near-IR spectra are found (Fig. 8), strong  $\text{H}_2\text{O}$  bands always implying large amplitude variability ( $\delta V > 1.7$  in our sample). None of the (quasi-)static M giants of the sample show impressive water vapour bands. This property has been qualitatively reproduced by first generations of models (Bessell et al. 1989a,b, 1996). As a result of pulsation, LPVs develop extended atmospheres with thicknesses comparable to the effective stellar radius (Wood 1979; Bowen 1988; Feuchtinger et al. 1993). Dense cool layers can exist, allowing  $\text{H}_2\text{O}$  and, at later stages, even dust to form. According to the pulsating star models used in Bessell et al. (1996) and Hofmann et al. (1998; relevant data kindly provided by M. Scholz), observations at the wavelengths of water vapour bands sample regions typically a factor of 1.4 – 2 further out in the atmosphere than observations in the quasi-continuum windows (e.g. at 2.2 or 1.04  $\mu\text{m}$ ). The shape of the water bands depends on details of the instantaneous atmospheric structure, which leaves much freedom to explain the variety of observed shapes and depths but makes it difficult to

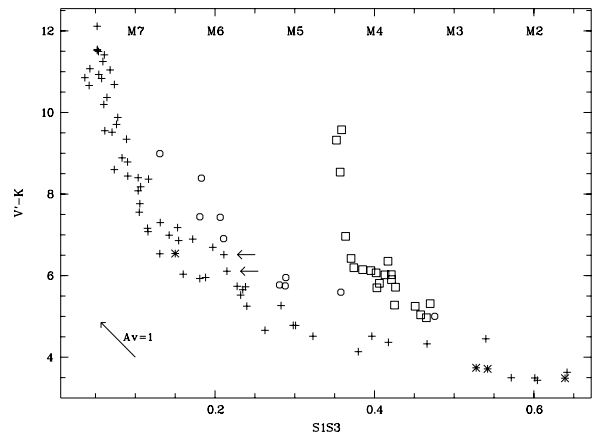


**Fig. 7.** The temperature sensitive broad band colour  $V' - K$  (cf. Sect. 2.4) plotted against the optical, spectral type sensitive index S1S3 (defined as  $S_{1/3,SP}$  in Fluks et al. 1994). Plus symbols represent both semi-regular and Mira-type O-rich LPVs; stars, circles and squares, respectively, are static giants, red supergiants and C-rich LPVs. Horizontal arrows identify the small amplitude variable KV Car (see text)

determine the cause for any particular empirical  $\text{H}_2\text{O}$  feature. Some LPV spectra can be relatively well reproduced by existing models, but for the same star the fits at other pulsation phases is often poor, casting doubt on the overall model reliability. Spectra with strong water vapour bands but otherwise warm energy distributions, such as S Car, have not as yet been reproduced by models (Mouhcine & Lançon 1999a; Matsuura et al. 1999).

Additional systematic differences between stars of various luminosity classes and variability types are described in Alvarez et al. (2000). While segregation tools are already available at the resolution of the present data, it is clear that higher resolution data would be helpful, in

particular in distinguishing between the various sources of opacity between 0.8 and 1.2  $\mu\text{m}$ .

### 3.3. Emission lines

Many miras are already classified as emission line stars in the GCVS on the basis of the Balmer line emission seen in the blue part of the spectrum. The most conspicuous near-IR emission line is Paschen  $\beta$ , which is located in a relatively clean spectral range, be it with respect to intrinsic stellar absorption bands or to telluric absorption. Equivalent widths of up to 6  $\text{\AA}$  are observed in our sample (RS Hor, March 1996, Fig. B13). Higher order lines of the Paschen series are fainter than  $P\beta$  and are located in stellar molecular bands of TiO and VO. Brackett  $\gamma$  is more difficult to recover and  $P\alpha$  completely lost because of telluric  $\text{H}_2\text{O}$  absorption (cf. Fig. 2).

Line emission in Miras is a transient phenomenon: there is no indication in our data that any star displays emission lines throughout its pulsation cycle, a fact already known from optical studies (e.g. Merrill 1940). GCVS phases are available for 25 stars in the sample; we have been able to replace them with more recent phase information only in a few cases of particular interest. Despite the uncertainties on the GCVS phases, the phase distribution of stars with emission lines shows a significant excess at phases 0.75–1 and a corresponding significant dip at phases 0.2–0.45, when compared to a uniform distribution. Models that incorporate shock formation and attenuation in LPV atmospheres predict that these shocks are strongest during the rising part of the light curve or around maximum light (Bessell et al. 1996). With the necessary caution due to limited phase information, the present data are consistent with a physical association between such shocks and the line emission (however, see e.g. Gillet 1988, for an alternative interpretation).

### 3.4. Metallicity

Only few theoretical studies exist of the effect of metallicity,  $Z$ , on near-IR spectra of luminous red stars with otherwise identical global properties (e.g.  $T_{\text{eff}}$ ,  $g$ , atmospheric extension, microturbulent velocity). The concept of metallicity itself is controversial, since several dredge-up episodes are likely to have modified the abundance ratios as compared to solar values.

Bessell et al. (1989a) studied the effect of metallicity on low resolution spectra of static stars. Their model spectra show that the effects of  $Z$ ,  $T_{\text{eff}}$  and  $g$  on spectrophotometric indices are highly degenerate (Lançon & Scholz, ongoing study).

Origlia et al. (1997), based on higher spectral resolution radiative transfer calculations and on static giant stellar structures with  $T_{\text{eff}} \geq 3000$  K, suggest that the equivalent width of the Si I line at 1.59  $\mu\text{m}$  provides a relatively

robust metallicity scale. The authors note, however, that the line is contaminated by OH in cooler stars (see also Fig. 6). The Al doublet at 1.316  $\mu\text{m}$  (Joyce et al. 1998), or metal features in the  $K$  band (Na 2.20  $\mu\text{m}$ , Ca 2.26  $\mu\text{m}$ ) may provide alternatives. The calibration of all the potential metallicity indicators remains challenging even for static giants, although progress is being made (Ramírez et al. 2000). In LPVs, the strong dependence of the many weak molecular lines on details of the instantaneous stellar structure affects the pseudo-continuum and makes the interpretation of metal lines even more complex.

Model independent insight into the effect of metallicity on LPV spectra can in principle be obtained by comparing stars known or suspected to belong to populations of established metallicities. LMC, SMC and thick disk or halo objects are expected to be metal deficient. S Car and S Lib, whose radial velocities approach 300  $\text{km s}^{-1}$  (Feast 1963), are both commonly associated with Population II or the thick disk. Figure 9 shows that very similar spectra can be found among the halo/thick disk and the LMC/SMC subsamples. Note, however, that HV 2360 is a supergiant with mass  $\sim 8 M_{\odot}$  and  $M_{\text{bol}} \sim -8.15$  (Wood et al. 1983) while S Car and S Lib presumably have  $M < M_{\odot}$  and  $M_{\text{bol}} \sim -4$  (from the  $M_{\text{bol}} - \log P$  relation of Hughes & Wood 1990). Relatively strong CN bandheads at 0.77, 0.92 and 1.1  $\text{\AA}$  in HV 2360 and the other LMC and SMC supergiants (Fig. B26) is consistent with the expectation that hot-bottom burning nucleosynthesis in these stars is converting carbon (probably dredged-up) into nitrogen. The number of matching pairs of spectra in the sample is too small to draw any final conclusion from these comparisons.

As a further step, we may use the metal lines mentioned earlier to attempt to identify metal-poor stars in the sample and then look for systematic spectral differences between these and the other objects. First, we note that the Na 2.20  $\mu\text{m}$  and Ca 2.26  $\mu\text{m}$  line blends of the large radial velocity objects S Car and S Lib are among the weakest of our sample. Taking weak Ca and Na lines as a tentative criterion for low metallicity, one is led to select the Magellanic Cloud stars as well as spectra of the SRa variables T Cen and BD Hya and the Miras RS Hor, RY CrA, SV Tel. Of these, T Cen has been previously associated with the halo or the thick disk by Alvarez et al. (1997; table in Alvarez 1997). Eye inspection (confirmed by colour measurements) shows that this list contains the hottest objects of the sample, illustrating the degeneracy between the effects of temperature and metallicity. All selected objects have periods below 225 days; reciprocally however, some short period SR variables fail to join the list, e.g. S Phe or SY Vel. The amplitudes of the selected objects range from 1.8 to 5.5 magnitudes in  $V$ , so that amplitude provides no further directly useful information for metallicity selection.

When concentrating on the spectra with weak metal lines, eye inspection suggests a systematically high

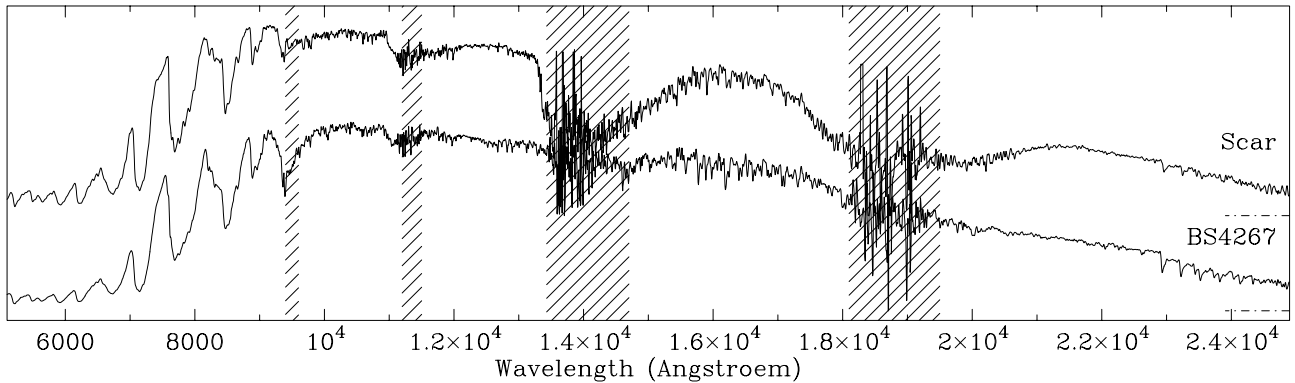


**Fig. 8.** The M 5 giant BS 4267 and the Mira-type LPV S Car (July 1996), two stars with similar optical spectra and large scale energy distribution. Note that water vapour absorption is much more prominent in the variable star S Car. Here and in subsequent spectral plots the dashed areas are those of very strong telluric absorption (season dependent, cf. Fig. 2), in which the signal-to-noise ratio after correction generally remains unacceptably low

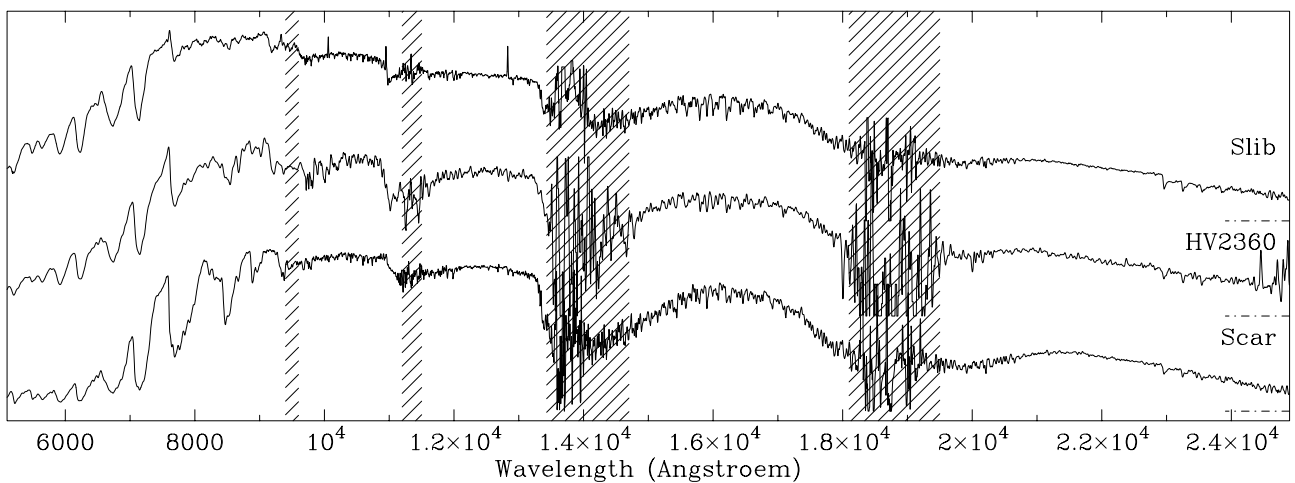


**Fig. 9.** The LMC star HV 2360 (smoothed) and the two galactic, high radial velocity Miras S Lib (May 1996) and S Car (July 1996)

$\text{H}_2\text{O}/\text{CO}$  absorption ratio. The trend is illustrated in Fig. 10. Despite their relatively blue colours, the stars selected tend to have strong water vapour bands. It is tempting to relate the high  $\text{H}_2\text{O}/\text{CO}$  absorption ratios to low metallicity, as the abundance of CO depends on the square of the heavy element abundance. However, as already mentioned, apparently weak metal lines can result from a depressed pseudo-continuum due to many enhanced molecular lines, and we may simply have *selected* relatively hot stars with particularly strong  $\text{H}_2\text{O}$  absorption. Only high resolution spectroscopy can solve this degeneracy.

Among the spectra with small Ca equivalent widths, those of S Lib stand out with relatively strong CO bands, a potential signature of a high C/O ratio (see discussion about SV Lib in Appendix A) or high luminosity. We note that S Lib is one of the few stars for which the automatic distance assignments of Alvarez et al. (1997), based respectively on optical and near-IR data, gave deviant results.

The relatively long period Bulge stars included in the sample (Fig. B25) are expected to be metal-rich. As discussed in Alvarez et al. (2000), the Bulge spectra are heavily reddened but are unlikely to be contaminated significantly by circumstellar dust emission. Once corrected for extinction, they generally remain redder than optically visible late-type AGB stars of the solar neighbourhood. Wood & Bessell (1983) interpreted this as the consequence of the lower effective temperatures of high metallicity AGB evolutionary tracks. Note, however, that dereddened Bulge spectra can be matched by the spectra of very late type Galaxy field LPVs (near minimum) very well (Fig. 11).

Perhaps we may use similarity to dereddened Bulge spectra as a selection criterion for metal-rich field stars. Some matching pairs are listed in Table 7. Obviously, using the Bulge stars of our sample as templates leads us to select only stars of the latest spectral types as potentially metal-rich stars.

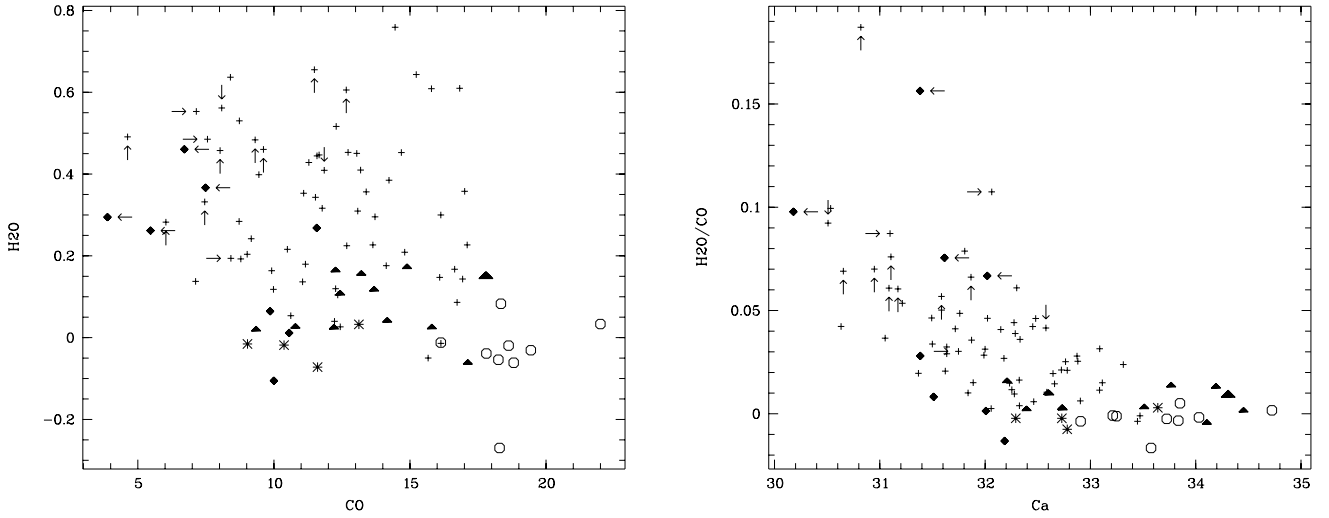


**Fig. 10.** Potential metallicity indicators. Left: an index measuring the absorption in the short wavelength wing of the  $1.9 \mu\text{m}$   $\text{H}_2\text{O}$  feature (in relative magnitudes), versus a measure of the equivalent width of the CO (2–0) bandhead at  $2.29 \mu\text{m}$  (arbitrary linear wavelength unit). Right: the ratio  $\text{H}_2\text{O}/\text{CO}$  of these absorption measures versus the equivalent width of the Ca line blend at  $2.26 \mu\text{m}$  (arbitrary linear wavelength unit). The symbols are as in Fig. 7, except that semi-regular variables are shown as triangles (SRb, SRc) and diamonds (SRa). Arrows identify 4 of the stars with weak Ca and Na line blends: S Car (pointing up), BD Hya (left), RY Cra (down) and RS Hor (right). The strengths of all features vary considerably. The coordinates of the two spectra of S Lib are (11.2, 0.18) and (9.9, 0.16) in the first graph, (31.4, 0.02) and (31.6, 0.02) in the second

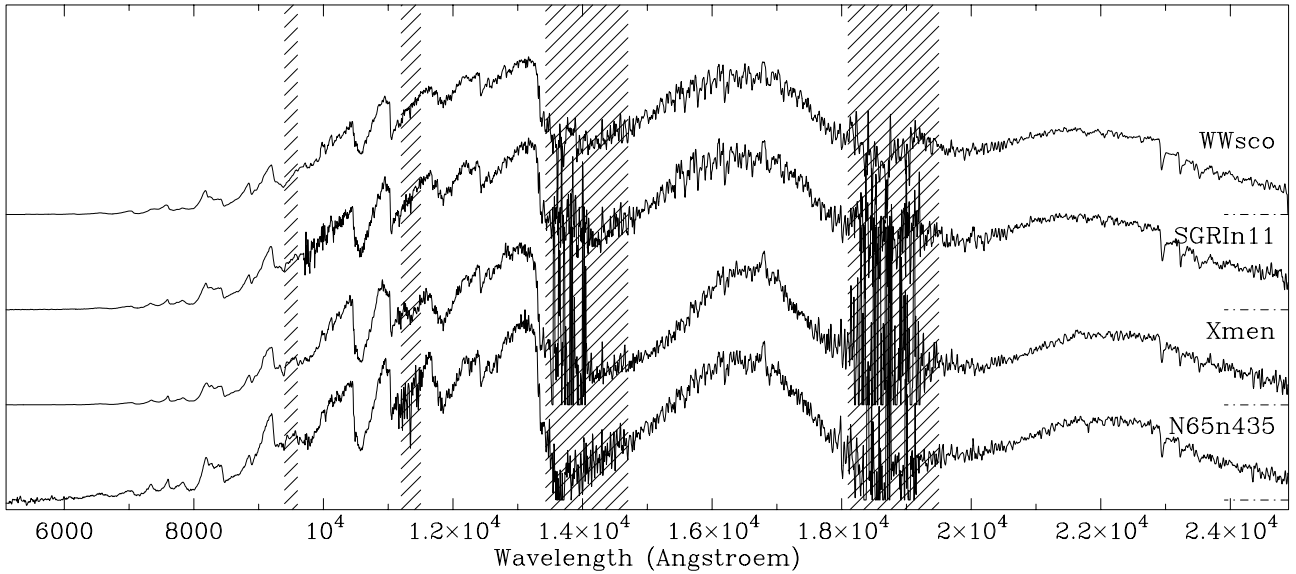


**Fig. 11.** Comparison between dereddened Bulge star spectra and spectra of Galaxy field stars (cf. Table 7)

**Table 7.**

Bulge spectrum	Reddening correction $E(B - V)$	Similar field star	Figures
NGC 6522 n435 (May 1996)	1.6	X Men (Mar. 1996)	B25, B19
NGC 6522 n426 (May 1996)	0.4	RS Lib (Jun. 1995)	B25, B18
NGC 6522 n205 (May 1996)	0.0	AFGL 1686 (Apr. 1995)	B25, B24
SGR In11 (Jul. 1996)	1.0	RS Hya (Feb. 1995)	B25, B15
SGR In11 (Jul. 1996)	0.5	WW Sco (Jun. 1995)	B25, B22

### 3.5. Variations

Figures B6–B31, each of which displays multiple spectra for the same star, show how spectra can vary with phase through the pulsation cycle. Note that the large  $V$  band amplitudes of many Miras are the result of variations of approximately one magnitude in bolometric light, combined with large changes in the bolometric correction  $BC_V$ . For S Car ( $\delta V = 6.6$ ), RS Hor ( $\delta V = 5.2$ ), RZ Car ( $\delta V = 6.2$ ) and RS Hya ( $\delta V = 5.2$ ) we find, respectively,  $\delta BC_V \geq 3.0, 3.7, 3.0$  and  $3.4$ . The spectra plotted per object in this paper illustrate the corresponding variations in colours and spectral signatures.

Alvarez & Plez (1998) illustrated clearly that optical signatures like the bands of TiO and VO both vary with phase but do not reach maximum depth at the same time. Similar variations and phase shifts are observed in the infrared. It has already been mentioned in Sect. 3.3 that the HI emission lines are strongest around or somewhat before maximum light.

An interesting new result suggested by the spectra is that CO and metal line absorption may be systematically reduced for a short time interval during the rising part of the light curve, around phase 0.7 (this is perhaps related to the line blurring and veiling noted in the blue spectra of Miras - see Merrill 1940). Searching for individual spectra with apparently reduced CO with respect to all other observations of the same star, we find: the June 1995 spectrum of RZ Car (GCVS phase 0.7, phase  $\sim 0.8$  according to the AAVSO bulletin, Mattei 1999; Fig. B8), the July 1996 spectrum of X Men (GCVS phase 0.7; Fig. B19), the June 1995 observation of R Phe (GCVS phase 0.62; Fig. B20), the June 1995 spectrum of S Car (GCVS phase 0.8, phase 0.7 – 0.75 according to the AAVSO bulletin and to AFOEV data (AFOEV 1999); Fig. B7) and the May 1996 observation of R Cha (GCVS phase 0.58,  $\sim 0.8$  according to the AAVSO bulletin 1999, Fig. B10). No spectrum with reduced CO was found at phases larger than 0.9 or smaller than 0.6. No spectrum with significantly enhanced CO (as compared to other phases of the same star) was found around phase 0.7. This phenomenon suggests that the atmosphere (or at least the relatively deep region of the photosphere responsible for the aspect of the CO bands and metal lines) goes through a particularly compact stage while luminosity increases, which is consistent with predictions from pulsation models (e.g. Bessell et al. 1996) in which a shock wave is starting to emerge from the deep layers around phase 0.7. At low resolution, it is not possible to investigate more subtle potential causes for the apparent weakening of the CO bands, such as line doubling or the superimposition of CO emission in the strongest lines (as discussed by Aringer et al. 1999, for SiO bands, or seen in U Equ, Fig. B24 and Appendix A).

Another example of delayed variation cycles is found in the 1 – 1.3  $\mu\text{m}$  range. Using the fluxes in the pseudo-continuum windows at 1.04 and 1.23  $\mu\text{m}$ , one can

identify a few spectra with particularly blue pseudo-continua in this range but otherwise cool energy distributions and clear VO absorption: RS Hor in Jan. 96 (Fig. B13), SV Tel in June 95 (Fig. B23), RS Hya in Apr. 96 (Fig. B15). All these spectra display HI emission, indicating that they were observed just before or around maximum light. Somewhat later observations in the same pulsation cycle (RS Hor in Mar. 96, RS Hya in May 96) show similar near-IR spectra, warmer optical spectra and no VO absorption. Again, this points to the existence of a brief moment shortly before maximum light during which the spectral properties originating in deeper layers indicate higher temperatures than the molecular features originating further out.

Pulsating Mira models without heavy mass loss (e.g. Bessell et al. 1996) predict non-periodic behaviour of the upper atmospheric regions so that there are cycle to cycle variations in these regions and in the location and strength of the shocks that run through them. Such changes lead to obvious spectral variations from cycle to cycle. As examples, we may cite:

— RS Hya (Fig. B15): the June 1995 spectrum has been obtained in an earlier cycle than the others (1.05 cycles before the May 1996 spectrum) and clearly displays much weaker H<sub>2</sub>O absorption;

— RZ Car (Fig. B8): deeper H<sub>2</sub>O absorption in the March 1996 observation than in the June 1995 spectrum, observed exactly one cycle earlier.

As expected, the most obvious cycle to cycle variations concern the H<sub>2</sub>O bands as these form in the upper cool layers whose structure is sensitive to details of the history of successive shock passages.

The well sampled light curve available for S Car (Fig. 12) allows us to highlight the intimate link between irregularities of the luminosity evolution and cycle-to-cycle variations in the spectra. The February 1995 and December 95 spectra, at the top of Fig. B7, were taken close to maximum light. A higher (optical) luminosity was reached in December than in February; the December data has weaker H<sub>2</sub>O features than its February counterpart. The July 96 and March 96 spectra, at the bottom of Fig. B7, correspond to minimum light. The March minimum had a lower luminosity than the July minimum; it shows very deep and broad H<sub>2</sub>O absorption and a clear VO band at 1.05  $\mu\text{m}$  that is absent in the July data. At a given phase, the strength of the molecular features and the current (optical) luminosity are clearly anticorrelated for this irregular Mira variable.

### 3.6. C stars

The spectra of carbon stars have little in common with those of oxygen-rich giants apart from CO absorption and a red energy distribution. Our sample (Figs. B28–B31) is relatively small. However, several general comments can be made.

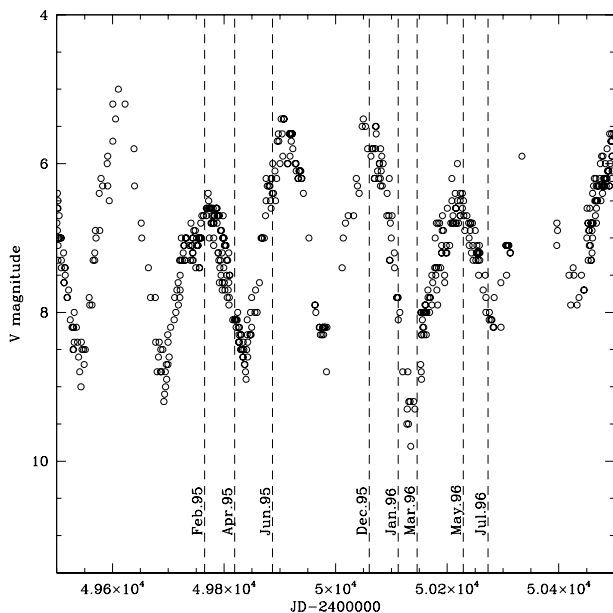


**Fig. 12.** Optical light curve of S Car. The AAVSO data plotted was kindly provided by J.A. Mattei in numerical form (we also acknowledge that AFOEV made similar data available to us). The acquisition dates of the spectra of Fig. B7 are indicated

As compared to O-rich stars, the spectra of C-rich LPVs tend to vary little with phase. O-rich LPVs with visual amplitudes of about 1.8 show significant changes, whereas the available C stars with similar amplitudes don't. The molecules that shape the near-IR spectrum of C stars, essentially CO, CN and C<sub>2</sub>, are formed deeper in the atmosphere than their counterparts in O-rich stars, TiO and H<sub>2</sub>O (Loidl et al. 2000); the influence of dynamics in deep layers is smaller. Stronger variations with phase are found at longer, mid-IR wavelengths, where the main molecular bands are due to molecules that form at lower temperatures, such as C<sub>2</sub>H<sub>2</sub>, HCN and C<sub>3</sub> (e.g. Hron et al. 1998). Note that the S/C star BH Cru and the cool, large amplitude ( $\delta V = 6.2$  mag) variable R Lep do exhibit significant near-IR variations (see Appendix A regarding peculiarities of R Lep).

Since the spectra of low amplitude C-rich LPVs are not very sensitive to pulsation, it is meaningful to compare them to theoretical spectra of static stars. A detailed comparison will be discussed by Loidl et al. (2000). Preliminary results are promising: the comparisons show that molecular line lists and their incorporation into the radiative transfer codes have made very significant progress in recent years and may now be satisfactory. The models indicate that the C/O ratio is a dominant factor in explaining star to star differences, and in particular the strength of the C<sub>2</sub> bandhead at 1.77  $\mu\text{m}$ . A C/O ratio of at least 1.4 is necessary to reproduce the bandheads observed in Y Hya or S Cen. Empirically, carbon stars

can easily be ordered into a sequence according to the ratio of the strengths of the C<sub>2</sub> bandhead at 1.77  $\mu\text{m}$  and various CO bandheads. The CO bands of the S/C star BH Cru are as strong as those of the coolest supergiant stars of our sample. Correspondingly, C<sub>2</sub> absorption in this object is weak.

An interesting feature of the C-rich spectra is the apparent absence of Si I absorption at 1.59  $\mu\text{m}$ . This empirical fact may simply be the result of blends with the many CN and C<sub>2</sub> lines, although the strong CO bandheads in the same spectral range don't seem to be affected. Alternatively, Si might be bound preferentially into silicon carbides. Within current theories for the formation of SiC grains (e.g. Kozasa et al. 1996) the condensation temperatures are low compared to the temperature required to populate the lower level of the Si I line, making this particular depletion mechanism unlikely; but silicon carbide formation theories are not yet final. OH lines are also absent in carbon star spectra, as expected if all oxygen is locked up in CO.

#### 4. Fundamental stellar parameters

If the spectra of this paper are to be used in association with population synthesis models, it is necessary to relate them to fundamental stellar parameters such as initial mass, initial metallicity and evolutionary status. Ideally, one should derive these parameters for each individual object and compute an energy-weighted mean spectrum to be used at one particular point of one particular AGB evolution track. As discussed by Lançon (1999), this currently isn't practical, be it only because it requires light curves and a full phase coverage for each star. Lançon et al. (1999) have adopted a different procedure based on averages inside apparent temperature bins instead of mean spectra of individual objects. The underlying assumptions and the required calibration of the resulting population synthesis predictions will be discussed in detail elsewhere (Mouhcine et al., in preparation). It remains useful to investigate the nature of the stars observed for this paper, because it will allow us to reevaluate the two procedures once more stellar and extragalactic data becomes available.

Optically visible Miras are observed to lie on a rather narrow period-luminosity (PL) relation (Feast et al. 1989; Hughes & Wood 1990) with little or no metallicity dependence. Even the effects of the O-rich to C-rich transition are small (Groenewegen & Whitelock 1996). A main result of the 5 year photometric survey of LMC stars by the MACHO consortium was the demonstration that large amplitude variables and a significant fraction of the semi-regular variables with *V* amplitudes larger than 1 mag are fundamental mode pulsators (Wood et al. 1999). Vassiliadis & Wood (1993) combined a theoretical fundamental mode period-mass-radius relation with stellar evolution models to compute the evolutionary tracks

**Table 8.** Indicative initial masses for variable stars, sorted by period, with the assumption of either LMC (lower value) or solar metallicity (higher value). Fundamental mode pulsation is assumed; overtone pulsation leads to higher masses (see text)

Star	vartype	$\delta V$	$P$	$M$	Notes
SY Vel	SRb	1.30	63.0	$\leq 0.94$	O
S Cen	SR	1.5	65	$\leq 0.94$	C
ET Vir	SRb	0.20	80.0	$\leq 0.94$	O
T Cen	SRa	3.50	90.4	$\leq 0.94$	P
BD Hya	SRa	1.80	117.4	$\sim 0.94$	P
Z Aql	M	6.60	129.2	$\sim 0.94$	
S Phe	SRb	2.00	141.0	$0.94 - 1$	
S Car	M	5.40	149.5	$0.94 - 1.1$	P
KV Car	SRb	0.80	150.0	$0.94 - 1.1$	O
T Cae	SR	1.80	156	$0.94 - 1.1$	C
U Crt	M	4.0	169.0	$0.94 - 1.2$	
AO Cen	M	1.90	189.0	$0.95 - 1.3$	
S Lib	M	5.50	192.9	$0.95 - 1.3$	P
RY Cra	M	1.90	195.0	$0.95 - 1.3$	P
RS Hor	M	5.20	202.9	$0.96 - 1.3$	P
RS Lib	M	6.0	217.6	$0.97 - 1.3$	R
SW Hya	M	3.20	218.8	$1 - 1.4$	
R Cir	SRb	1.90	222.0	$1 - 1.4$	
SV Tel	M	3.00	225.5	$1 - 1.5$	P
V 603 Cen	M	2.30	253.0	$1 - 1.6$	
UZ Hya	M	5.70	261.0	$1.1 - 1.7$	
R Phe	M	6.90	269.3	$1.1 - 1.7$	
RZ Car	M	6.2	272.8	$1.1 - 1.7$	
V Oph	M	4.3	297.2	$1.25 - 1.9$	C
Z Lib	M	3.60	298.6	$1.25 - 1.9$	
Y Hya	SRb	3.70	302.8	$1.25 - 1.9$	C
R Leo	M	6.9	312.0	$1.3 - 1.95$	
R Cha	M	6.7	334.6	$1.5 - 2.1$	
CM Car	M	2.50	335.0	$1.5 - 2.1$	
RS Hya	M	5.20	338.6	$1.5 - 2.1$	R
EV Car	SRb	1.40	347.0	$1.55 - 2.2$	
DX Ser	SRa	2.00	360.0	$1.65 - 2.25$	
R Cnc	M	5.6	361.7	$1.65 - 2.25$	
X Men	M	3.60	380.0	$1.8 - 2.4$	R
SV Lib	M	1.30	402.7	$2 - 2.5$	
BH Cru	M	2.8	520.0	$2.2 - 2.6$	C
RU Pup	SRb	1.90	425	$2.2 - 2.65$	C
R Lep	M	6.20	427.1	$2.3 - 2.7$	C, IR
WW Sco	M	4.1	431.0	$2.3 - 2.7$	R
CL Car	SRc	2.50	513.0	$3.3 - 3.7$	S
WX Psc	M	$>2.5$	645	$> 5$	
AFGL 1686	M	$>2.5$	700:	$> 5$	IR

Notes to Table 8:

O: overtone pulsator? C: carbon rich star. P: metal poor? R: metal rich? IR: IRAS source. S: supergiant.

of TPAGB stars in the PL diagram. Assuming that the stars of our programme lie on the mean Mira PL relation, we have used these tracks to estimate the stellar initial masses. The PL evolution of a TPAGB star depends on metallicity: at a given luminosity and for a given initial mass, a metal rich star will have a lower effective temperature due to higher opacities and a smaller mass due to enhanced mass loss, two effects that combine to lengthen the pulsation period. Table 8 lists the initial masses derived assuming either LMC or solar metallicity.

In Sect. 3.4, potentially metal poor or metal rich stars have been identified. Due to the global chemical evolution of the solar neighbourhood, a general correlation between age and metallicity exists: with the above assumption of a single mode of pulsation, stars with short periods have

low initial masses and are thus likely to be metal poor (the smaller of the mass estimates of Table 8 is more appropriate), while stars with long periods are more massive, thus younger and more metal rich (i.e. the larger of the mass estimates applies).

On the other hand, a subsample of the small amplitude, short period LPVs may be overtone pulsators. Surveys show that additional PL sequences run parallel to the Mira sequence on the high luminosity side, consistent with overtone pulsation (Bedding & Zijlstra 1998; Wood et al. 1999). These sequences are populated with semi-regular variables, mostly with  $V$  band amplitudes smaller than  $\sim 1$  magnitude and periods shorter than 200 days. Higher initial masses (and an earlier evolutionary status) would result from the use of the corresponding PL relations. The only stars this may reasonably apply to in our sample are ET Vir, SY Vel and KV Car. As an example, the 150 day period of KV Car would suggest an initial mass of the order of  $2 M_{\odot}$  if overtone pulsation applied, instead of about  $1 M_{\odot}$  in the case of the fundamental mode assumption. The resulting high luminosity might then explain the relatively strong CO bands of KV Car noted in Sect. 3.2.

The longest period variables of the sample are IRAS sources, i.e. they are losing mass at superwind rates and lie on the long period side of the mean PL relation of optically visible Miras. At this stage of evolution, the periods increase rapidly and the tracks run horizontally in the PL diagram for all initial masses. The spectra of the IRAS sources thus probably correspond to late stages of stars slightly less massive than indicated in Table 8.

## 5. Conclusion

We have presented digital spectra covering the spectral range from  $0.5$  to  $2.5 \mu\text{m}$  for a large sample luminous cool stars. The amazing variety of spectral properties found in the sample and the strong variations seen with phase in variable stars illustrate the sensitivity of many molecular features to the detailed structure of the atmosphere. Features such as the water vapour bands are particularly strong in variable stars, as compared to (quasi-)static giants, because of the atmospheric extension pulsation leads to. Frequent cycle-to-cycle variations make it compulsory to obtain complete data sets simultaneously, as it was done here, if the data are to be compared with model predictions or used for classification.

Although correlations exist between spectral properties and dynamical properties such as period and amplitude, they show a large dispersion. A more complete phase coverage of the pulsation cycle and, simply, a better phase and instantaneous luminosity information for the available data would help clarifying these relationships. The work of amateur astronomers in organisations such as the AAVSO and AFOEV will hopefully continue to provide such invaluable information.

The spectra of this paper may be used for population synthesis purposes. Methods, predictions and the necessary empirical calibration of the model predictions are discussed elsewhere (Lançon et al. 1999; Mouhcine & Lançon 2000; Mouhcine et al., in preparation).

*Acknowledgements.* This work made extensive use of the Simbad and Vizier literature search tools, operated at CDS, Strasbourg. We sincerely thank P. McGregor for invaluable help with IR observations in general and the analysis of CASPIR data in particular; we have also greatly appreciated the help of the MSSSO observer support team and computing section. A.L. thanks L. d'Hendécourt for helpful discussions on candidate chemical species for the  $1.53\ \mu\text{m}$  feature in R Lep.

## References

- Association Française des Observateurs d'Étoiles Variables (AFOEV), 1999, database accessible at <http://cdsweb.u-strasbg.fr/afoev/> under the responsibility of E. Schweitzer
- Alvarez R., 1997, Ph.D. Thesis, Étude des variables à longue période de type Mira dans le proche infrarouge, Université Paris VII, 27/11/1997
- Alvarez R., Plez B., 1998, *A&A* 330, 1109
- Alvarez R., Mennessier M.-O., Barthès D., Luri X., Mattei J.A., 1997, *A&A* 327, 656
- Alvarez R., Lançon A., Plez B., Wood P.R., 2000, *A&A* 353, 322
- Aringer B., Höfner S., Wiedemann G., et al., 1999, *A&A* 342, 799
- Barnbaum C., Omont A., Morris M., 1996, *A&A* 310, 259
- Bedding T.R., Zijlstra A.A., 1998, *ApJ* 506, L47
- Bedding T.R., Conn B.C., Zijlstra A.A., 2000, in: Szabados L., Kurtz D.W. (eds.), *The Impact of Large-Scale Surveys on Pulsating Star Research*, IAU Coll. 176, ASP Conf. Ser. (in press) ASP, San Francisco
- Bessell M.S., 1998, in: Bedding T.R., Booth A.J., Davis J. (eds.), *Fundamental stellar properties: the interaction between observation and theory*, IAU Symp. 189, 127
- Bessell M.S., Brett J.M., Scholz M., Wood P.R., 1989a, *A&AS* 77, 1
- Bessell M.S., Brett J.M., Scholz M., Wood P.R., 1989b, *A&A* 213, 209
- Bessell M.S., Brett J.M., Scholz M., Wood P.R., 1991, *A&AS* 89, 335
- Bessell M.S., Scholz M., Wood P.R., 1996, *A&A* 307, 481
- Bessell M., Castelli F., Plez B., 1998, *A&A* 337, 321
- Bowen G.H., 1988, *ApJ* 329, 299
- Bressan A., Chiosi C., Fagotto F., 1994, *ApJS* 94, 63
- Bressan A., Granato G.L., Silva L., 1998, *A&A* 332, 135
- Brett J.M., 1989, *MNRAS* 241, 247
- Brett J.M., 1990, *A&A* 231, 440
- Cardelli J.A., Clayton G.C., Mathis J.S., 1989, *ApJ* 345, 245
- Castelli F., Gratton R.G., Kurucz R.L., 1997, *A&A* 318, 841
- Charlot S., Bruzual G., 1991, *ApJ* 367, 126
- Cuntz M., Luttermoser D., 1990, *ApJ* 353, L39
- Dachs J., Wamsteker W., 1982, *A&A* 107, 240
- Doty S.D., Leung C.M., 1998, *ApJ* 502, 898
- Dyck H.M., Benson J.A., van Belle G.T., Ridgway S.T., 1996, *AJ* 111, 1705
- Eyer L., Grenon M., 1997, in: Battrick B. (ed.), *Proc. of the ESA Symp. Hipparcos – Venice '97*, ESA publ. SP-402, p. 467
- Feast M.W., 1963, *MNRAS* 125, 27
- Feast M.W., Glass I.S., Whitelock P.A., Catchpole R.M., 1989, *MNRAS* 241, 375
- Feuchtinger M.U., Dorfi E.A., Höfner S., 1993, *A&A* 273, 513
- Flower P.J., 1977, *A&A* 54, 31
- Fluks M.A., Plez B., Thé P.S., et al., 1994, *A&AS* 105, 311
- Gillet D., 1988, *A&A* 192, 206
- Girardi L., Bertelli G., 1998, *MNRAS* 300, 533
- Goebel J.H., Bregman J.D., Witteborn F.C., Taylor B.J., 1981, *ApJ* 246, 455
- Goebel J.H., Bregman J.D., Cooper D.M., et al., 1983, *ApJ* 270, 190
- Groenewegen M.A.T., Whitelock P.A., 1996, *MNRAS* 281, 1347
- Hanson M.M., Conti P.S., Rieke M.J., 1996, *ApJS* 107, 281
- Hauschildt P.H., Allard F., Ferguson J., Baron E., Alexander D., 1999, *ApJ* 525, 871
- Helling C., Jørgensen U.G., Plez B., Johnson H.R., 1996, *A&A* 315, 194
- Höfner S., Jørgensen U.G., Loidl R., Aringer B., 1998, *A&A* 340, 497
- Hofmann K.-H., Scholz M., Wood P.R., 1998, *A&A* 339, 846
- Hron J., Loidl R., Höfner S., et al., 1998, *A&A* 335, L69
- Hughes S.M.G., Wood P.R., 1990, *AJ* 99, 784
- Johnson H.J., Méndez M.E., 1970, *AJ* 75, 785
- Jones T.J., Bryja C.O., Gehrz R.D., et al., 1990, *ApJS* 74, 785
- Josselin E., Loup C., Omont A., et al., 1998, *A&AS* 129, 45
- Joyce R.R., 1998, *ApJ* 115, 2059
- Joyce R.R., Hinkle K.H., Wallace L., Dulick M., Lambert D.L., 1998, *AJ* 116, 2520
- Keady J.J., Hinkle K.H., 1988, *ApJ* 331, 539
- Kholopov P.N., Samus' N.N., Frolov M.S., et al., 1988, *General Catalogue of Variable Stars*, 4th Edition. Nauka Publ. House, Moscow
- Kipper T., 1998, *Balt. A.* 7, 435
- Kleinmann S.G., Hall D.N.B., 1986, *ApJS* 62, 501
- Kozasa T., Dorschner J., Henning T., Stognienko R., 1996, *A&A* 307, 551
- Kurucz, 1993, CDrom Number 13 (provided by the author)
- Lançon A., 1999, in: Le Bertre T., Lèbre A., Waelkens C. (eds.), *IAU Symp. 191, Asymptotic Giant Branch Stars*. ASP, San Francisco, p. 579
- Lançon A., Mouhcine M., Fioc M., Silva D., 1999, *A&A* 344, L21
- Lejeune Th., Cuisinier F., Buser R., 1997, *A&AS* 125, 229
- Lewis B.M., 1997, *ApJS* 109, 489
- Lloyd Evans T., 1976, *MNRAS* 174, 169
- Loidl R., Höfner S., Jørgensen U.G., Aringer B., 1999, *A&A* 342, 531
- Loidl R., Lançon A., Jørgensen U.G., 2000 (in preparation)
- Maiolino R., Rieke G.H., Rieke M.J., 1996, *AJ* 111, 537
- Maraston C., 1998, *MNRAS* 300, 872
- Marigo P., Girardi L., Bressan A., 1999, *A&A* 344, 123
- Matsuura M., Yamamura I., Murakami H., Freund M.M., Tanaka M., 1999, *A&A* 348, 579
- Mattei J.A., 1999, *American Association of Variable Star Observers (AAVSO) Bulletin* 62

- McGregor P., 1994, CASPIR manual, available at <http://msowww.anu.edu.au/> Research School for Astronomy and Astrophysics, Mount Stromlo Observatory, Canberra
- Merrill P.W., 1940, *Spectra of Long-Period Variable Stars*. Chicago: University of Chicago Press
- Morris S., Wyller A.A., 1967, *ApJ* 150, 877
- Mouhcine M., Lançon A., 1999a, in: Hubeny I., Heap S., Cornett R. (eds.), *Age Dating Stellar Populations*, ASP Conf. Ser. 192, 303
- Mouhcine M., Lançon A., 1999b, in: Hubeny I., Heap S., Cornett R. (eds.), *Age Dating Stellar Populations*, ASP Conf. Ser. 192, 113
- Mouhcine M., Lançon A., 2000, in: Lançon A., Boily C. (eds.), *Massive Stellar Clusters*, ASP Conf. Ser. 211, 144
- Neckel T., Klare G., Sarcander M., 1980, *A&AS* 42, 251
- O'Brien G.T. Jr., Lambert D.L., 1986, *ApJS* 62, 899
- Origlia L., Moorwood A.F.M., Oliva E., 1993, *A&A* 280, 536
- Origlia L., Ferraro F.R., Fusi Pecci F., Oliva E., 1997, *A&A* 321, 859
- Phillips J.G., 1969, *ApJ* 157, 449
- Ramírez S.V., Stephens A., Frogel J.A., DePoy D.L., 2000 (in preparation)
- Scalo J., 1973, *ApJ* 184, 801
- Shaw S.J., Bord D.J., 1990, *AJ* 99, 917
- Theodossiou E., 1985, *MNRAS* 214, 327
- Turnshek D.E., Turnshek D.A., Craine E.R., Boeshaar P.C., 1985, *An Atlas of Digital Spectra of Cool Stars*, A&AS Western Research Company
- Valenti J.A., Piskunov N., Johns-Krull C.M., 1998, *ApJ* 498, 851
- Vassiliadis E., Wood P.R., 1993, *ApJ* 413, 641
- Wallace L., Hinkle K., 1997, *ApJS* 111, 445
- Wood P.R., 1979, *ApJ* 227, 220
- Wood P.R., Bessell M.S., 1983, *ApJ* 265, 748
- Wood P.R., Bessell M.S., Fox M.W., 1983, *ApJ* 272, 99
- Wood P.R. and the MACHO Collaboration 1999, in: Le Bertre T., Lèbre A., Waelkens C. (eds.), *Asymptotic Giant Branch Stars*, IAU Symp. 191. ASP, San Francisco, p. 151
- Zirin H., 1982, *ApJ* 260, 655

## Appendix A: Comments on individual stars

### CL Car (Fig. B3)

In the GCVS, CL Car is classified as an LPV of variability SRc and spectral type M5Ia. Its spectrum indeed fits very well into the supergiant sequence, but it has relatively deep H<sub>2</sub>O bands in addition to CN absorption, probably a consequence of pulsation (period = 513 days, amplitude  $\delta V = 2.5$  mag). These properties already make CL Car interesting as a particularly large amplitude red supergiant or alternatively as a particularly massive Mira.

A remarkable feature of this luminous late-type star is the strong absorption line at 1.083  $\mu\text{m}$ , the wavelength of the transition between the triplet levels 2<sup>3</sup>S and 2<sup>3</sup>P of He I. The feature has an equivalent width of a few Å and is not an artifact since it is seen in all individual

raw and reduced spectra of the object and in no other spectrum of the same programme. Searches for He I absorption in this line in various types of cool stars have been reported by Zirin (1982) and O'Brien & Lambert (1986). Zirin concluded that absorption was rare in giants and supergiants later than type K3 except for symbiotic stars like Z And and R Aqr; CL Car might thus be a symbiotic star. With a better signal to noise ratio, O'Brien & Lambert found weak absorption in all K supergiants but no absorption in stars later than M1I. Note that only a few luminous M stars were observed in each of the samples.

No significant absorption is seen in the 2.058  $\mu\text{m}$  2<sup>1</sup>S – 2<sup>1</sup>P transition of He I in CL Car (although this line is located in a telluric CO<sub>2</sub> band which degrades the signal-to-noise ratio). The lower level of the 1.083  $\mu\text{m}$  transition of helium lies 626 Å above ground level, but is metastable as opposed to the lower level of the other near-IR transition at 2.058  $\mu\text{m}$  (2<sup>1</sup>S). Interpretations for the population of the 2<sup>3</sup>S level of He I in non-coronal stars range from X-ray photoionization through collisional excitation by thermal electrons to stochastic shock waves (Cuntz & Luttermoser 1990). In the latter mechanism, outwards running shock fronts initiated with various velocities merge and build up, possibly leading to temperatures above 20 000 K. Similar merging processes of successive shock waves are predicted to occur in Miras, but no 1.083  $\mu\text{m}$  absorption has been observed in any of those stars.

### U Equ (Fig. B24)

The observation of U Equ (= IRAS 20547+0247) was suggested by A. Omont. This heavily obscured object has recently revealed strong peculiarities (Barnbaum et al. 1996): the spectral type of the obscured star could range from mid-G to early-K, the optical spectrum indicates the luminosity class of a giant but shows anomalously deep and narrow molecular absorption lines of TiO, AlO and VO as well as bright molecular emission lines of the same compounds. The 12 – 25  $\mu\text{m}$  energy distribution indicates optically thin dust, while silicate absorption and a strong 60  $\mu\text{m}$  excess are consistent with a thick dust envelope. OH and H<sub>2</sub>O maser emission are present and highly variable (see also Lewis 1997). Circumstellar CO(2–1) emission has also been detected (Josselin et al. 1998). A non-spherical geometry seems necessary to account for all properties; Barnbaum et al. (1996) suggested the presence of a cold disk viewed nearly edge-on.

The 1.6 – 2.45  $\mu\text{m}$  spectrum obtained in May 1996 (Fig. B24) has a red slope consistent with the photometry collected in Barnbaum et al. (1996). H<sub>2</sub>O absorption is weak and narrow as compared to normal pulsating OH/IR stars. It is remarkable that no 2nd overtone CO absorption is detected longward of

2.29  $\mu\text{m}$ : the bands seem to be filled up with CO emission. A similar filling of molecular bands usually seen in absorption has been observed in the mid-IR with the Infrared Space Observatory (A. Omont, private communication).

### R Lep (Fig. B31)

R Lep is a transition object between optically visible and dust-enshrouded C-rich Mira variables. In addition to its red colours, two particularities of this object are worth notice: the presence of an absorption feature at 1.53  $\mu\text{m}$ , not seen in other (warmer) carbon stars, and the significant variations of the spectrum with phase. The four spectra obtained in 1995 and 1996 (GCVS phases 0.7 – 0.9, but  $\sim 0.4$  – 0.7 according to AAVSO data, Mattei 1999) drew our attention to the relatively broad absorption feature centered at 1.53  $\mu\text{m}$ . In order to check the phase dependence of the band, an additional spectrum was obtained in November 1997. The presence of the feature was confirmed (Fig. A1), and its strength found to have changed very little.

The 1.53  $\mu\text{m}$  feature has been previously noticed in a few low temperature carbon-rich Miras including V CrB, S Cep, U Cyg and SS Vir (Goebel et al. 1981) and V Cyg (Joyce 1998). Goebel et al. (1981) suggest HCN or C<sub>2</sub>H<sub>2</sub> as the main carriers. Joyce (1998) also favours this interpretation, noting that the presence of the 1.53  $\mu\text{m}$  band in a spectrum is associated with absorption around 2.45  $\mu\text{m}$ , as expected from the laboratory spectrum of C<sub>2</sub>H<sub>2</sub> (Goebel et al. 1981). However, HCN or C<sub>2</sub>H<sub>2</sub> are also responsible for the 3.1  $\mu\text{m}$  and no clear correlation with the 1.53  $\mu\text{m}$  feature is found (Joyce 1998). Chemical equilibrium networks for C-rich atmospheres (Morris & Wyller 1967; Scalo 1973; Helling et al. 1996; Doty & Leung 1998) predict that under adequate circumstances a large variety of carbon bearing molecules may be abundant. In addition to the most obvious C<sub>2</sub>, CN, HCN, CO, C<sub>3</sub> and C<sub>2</sub>H<sub>2</sub>, the species produced at low temperatures include C<sub>2</sub>H, CH<sub>3</sub>, C<sup>+</sup> and more complex compounds. Goebel et al. (1983) suggest C<sub>2</sub>H as the carrier of the 2.9  $\mu\text{m}$  band seen in the R type carbon star HD 19557. They present a theoretical spectrum which, taking into account the uncertainties on the predicted wavelengths as estimated by the authors, could explain the 1.53  $\mu\text{m}$  feature. The existence of C<sub>2</sub>H in cool carbon stars is further supported by the high resolution spectrum of IRC +10216 around 2  $\mu\text{m}$ , published by Keady & Hinkle (1998). Indirectly, the failure to reproduce the spectrum of V CrB with a network including HCN and C<sub>2</sub>H<sub>2</sub> but neglecting C<sub>2</sub>H enhances the probable role of the latter (e.g. Kipper 1998). Unfortunately, C<sub>2</sub>H is not included in most current spectral synthesis codes for carbon stars, because of lacking accurate chemical data (Hron et al. 1998; Plez et al., private communications).

Among our C-rich sample, R Lep is the only star displaying strong variations with phase. Circumstellar extinction may be significant for this object and it may possibly vary with phase; however, photospheric variations are required to explain the changes in the strengths of the CN bandheads at 1.1 and 1.4  $\mu\text{m}$ . The C<sub>2</sub> Ballik-Ramsay bandhead (1.77  $\mu\text{m}$ ) and the CO band strengths vary little in comparison. They are similar to those of the S/C Mira BH Cru (Fig. A1), indicating a relatively low C/O ratio for a carbon star. The efforts put into modelling the variations of cool C-stars in the ISO wavelength range need to be extended to the range of this data, in order to provide basic interpretation tools.

### SV Lib (Fig. B5)

This O-rich star displays a remarkably clean CO spectrum between 1.55 and 1.7  $\mu\text{m}$ . OH lines and the Si line at 1.59  $\mu\text{m}$  are particularly weak, similar to the S/C Mira BH Cru in this respect (Fig. A2). However, the star displays H<sub>2</sub>O absorption bands, normal VO absorption bands for its energy distribution and normal/strong TiO bands (Alvarez et al. 2000).

All three IK spectra available in the sample display P $\beta$  in emission: they are obtained close to maximum light, though in different cycles. The optical spectrum obtained in March 1996 is cooler by some 200 K (Alvarez et al. 2000). Near-IR observations at shorter time intervals are necessary to find out whether the weak-lined *H* band spectrum is a usual property of the star (possibly a relatively large C/O ratio) or whether it is peculiar to phases around maximum light.

Unfortunately the present observations do not allow us to constrain the rather uncertain pulsation properties of SV Lib. The GCVS indicates  $P = 402.7$  and  $\delta V \geq 1.3$ ; Shawl & Bord (1990) correct the period to 192 days (but mention aliases at 126 and 410 days in their data), and find an optical pulsation amplitude of about 5 mag. As shown in the following table, which lists the phases of the available spectra according to both references, the lack of data between June 95 and March 96 prevents a final conclusion.

Date	Phase	
	GCVS	B&S90
June 95	0.80	0.80
March 96	0.46	0.18
May 96	0.67	0.63
July 96	0.77	0.84

The understanding of pulsating atmospheres is not good enough to allow us to distinguish between phase 0.46 and 0.18 from an optical spectrum alone. The low flux level of the March 96 spectrum as well as the drop in effective temperature for this spectrum appear rather large and tend to favour the longer, GCVS period.

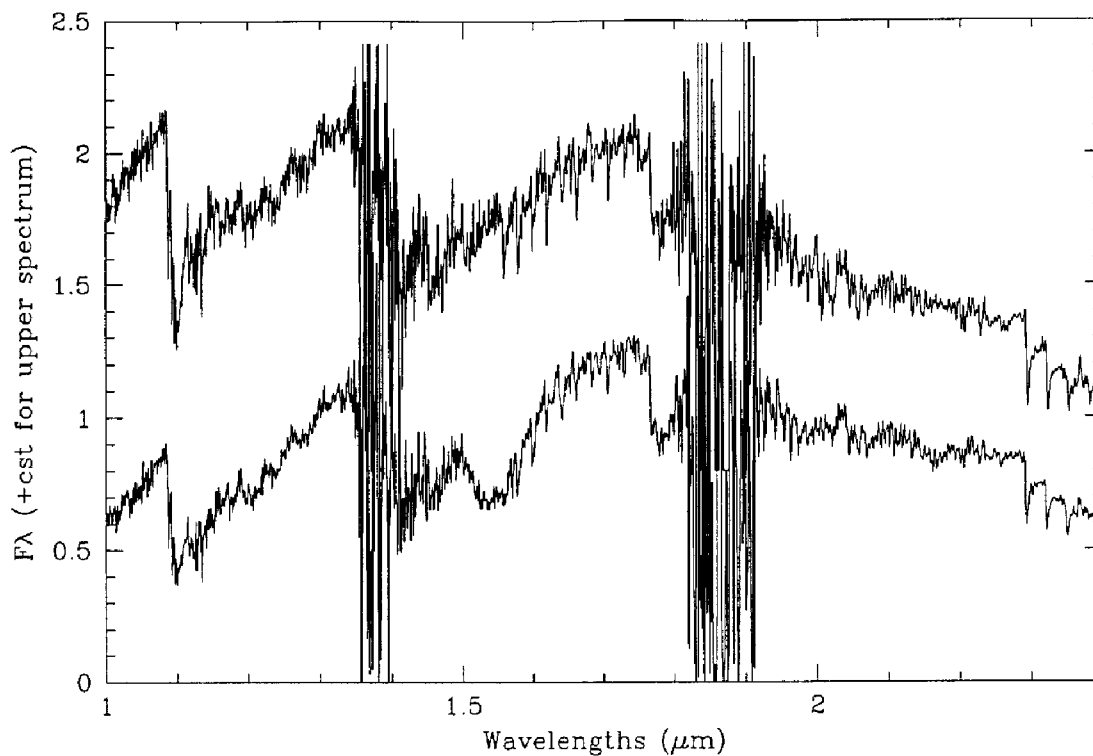


Fig. A1. R Lep (November 1997; bottom) and BH Cru (May 1996)

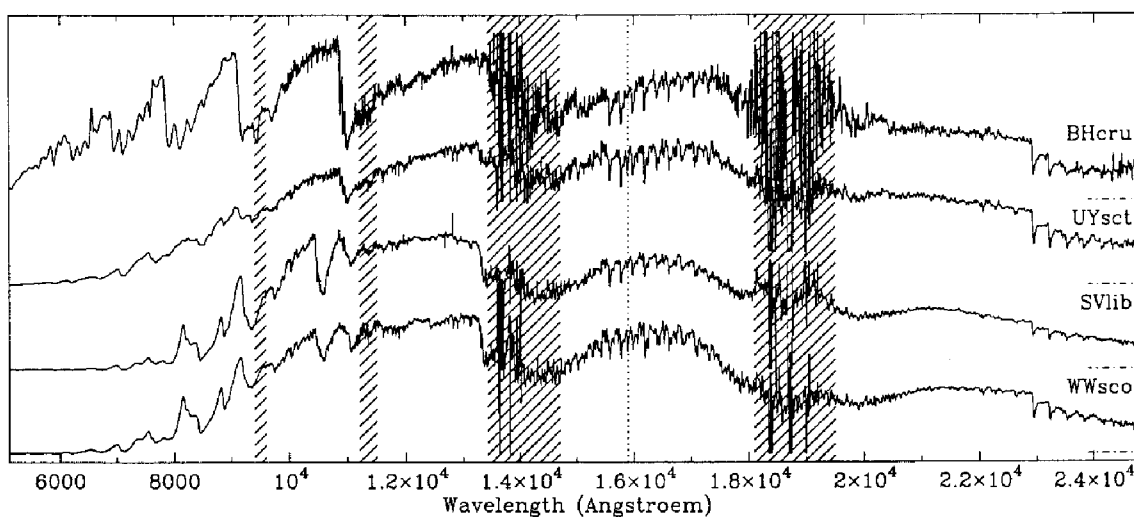
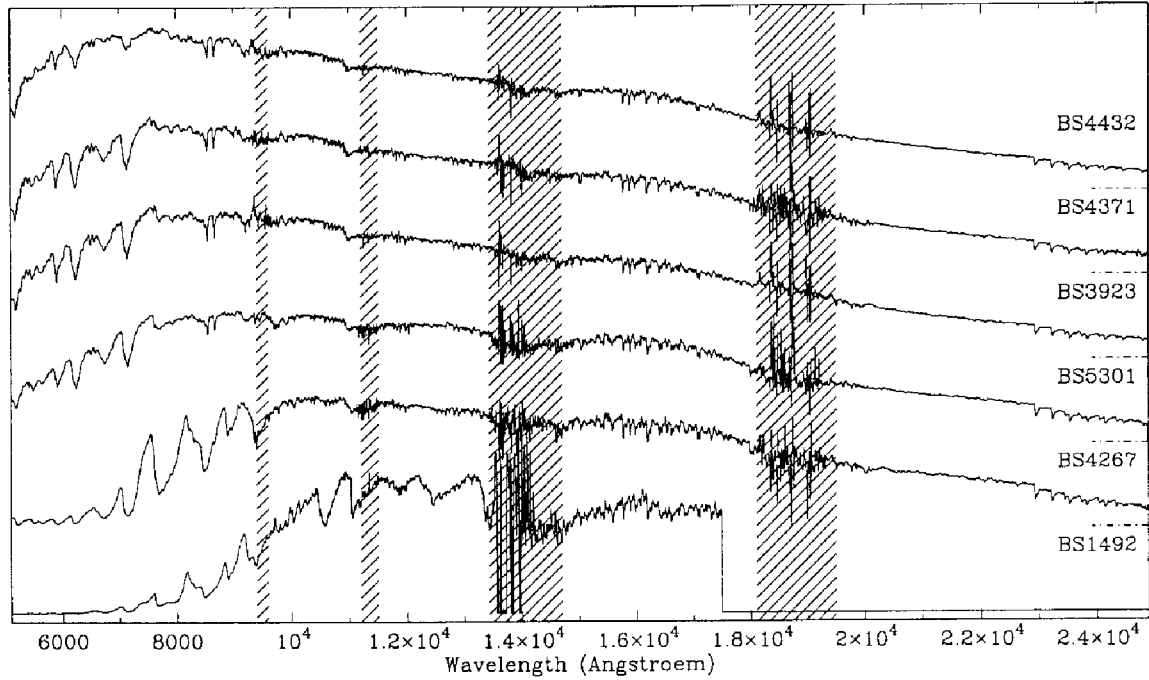


Fig. A2. The spectrum of SV Lib (May 1996, but all available data are similar), compared to the Mira variable WW Sco (May 1996), the cool supergiant UY Sct (May 1996) and the S/C Mira BH Cru (Jan. 1996). The position of the  $1.59 \mu\text{m}$  Si I line (blended with OH lines in cool O-rich objects) is indicated

## Appendix B: Spectra

### B.1. Giants and supergiants



**Fig. B1.** Static (or very low amplitude variable) giant stars. BS4432: K4.5; BS4371: M0; BS3923: M1, BS5301: M2 (= ET Vir, SRb,  $\delta V = 0.2$ ,  $P = 80$ ), BS4267: M5; BS1492: M8 (= R Dor, SRb,  $\delta V = 1$ ). Due to partial saturation of the detector during the observation of R Dor, the apparently strong and unusually shaped TiO absorption at  $1.25 \mu\text{m}$  and the dip around  $1.65 \mu\text{m}$  require confirmation. Shaded areas are those that could not (in general) be corrected for telluric absorption in a satisfactory way

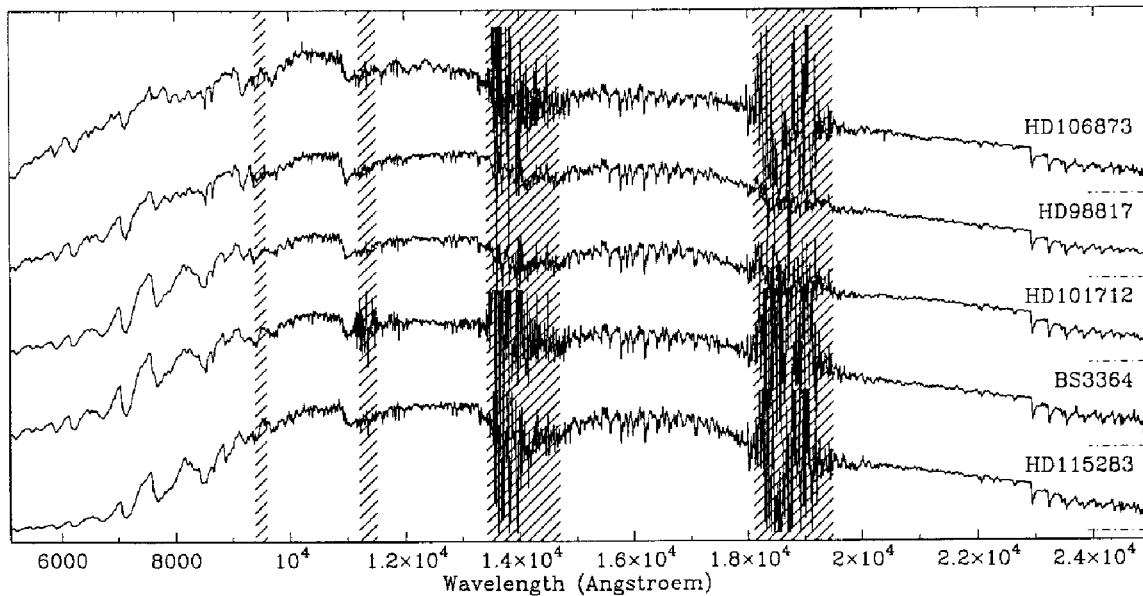


**Fig. B2.** Supergiant stars. Spectral types from the literature are, from top to bottom are: M0I, M1I, M2-3I, M2I, M4I

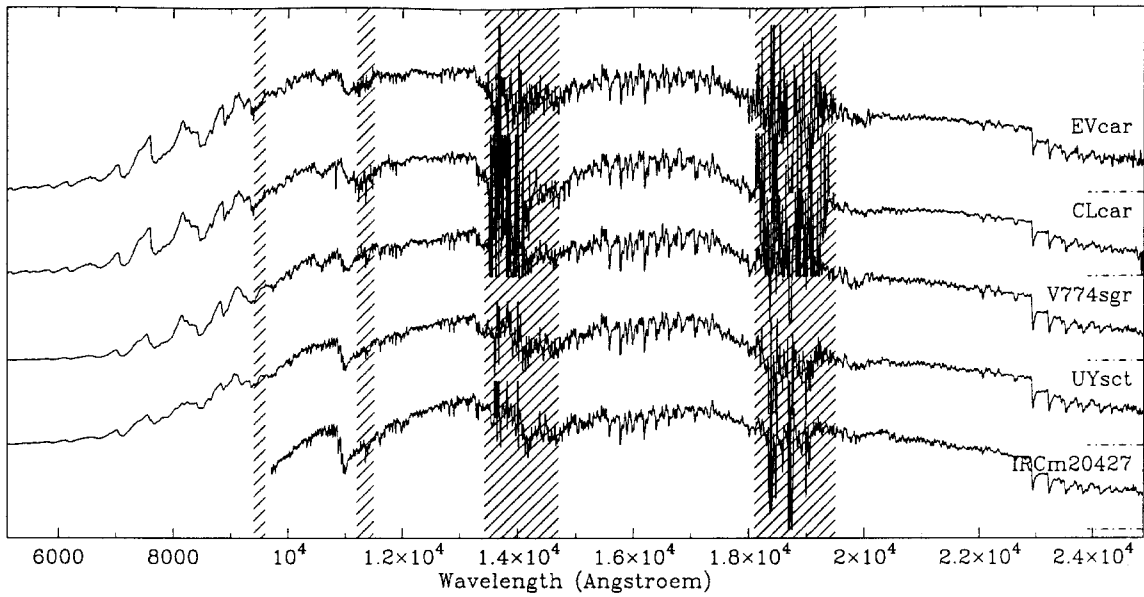


**Fig. B3.** Supergiant stars. Spectral types from the literature are, from top to bottom are: M4.5I, M5I, M4-5I, M4I, M3-4I. UY Sct, V774 Sgr, CL Car and EV Car are known low amplitude semi-regular variables. The absorption line near  $1.08 \mu\text{m}$  in CL Car is real

*B.2. Small amplitude O-rich LPVs*

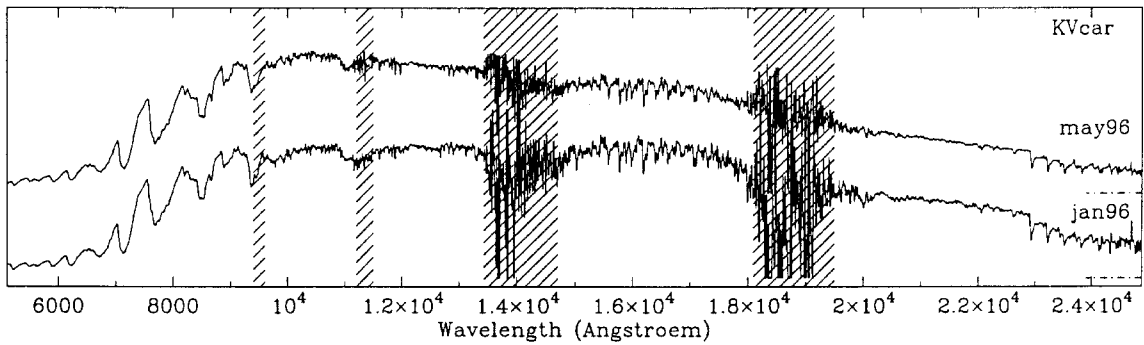


**Fig. B4.** KV Car:  $P = 150.0$ ,  $\delta V = 0.8$ . For display purposes, the spectra with the coolest energy distribution are placed at the bottom, the hottest ones at the top (here and in all further graphs). As for SY Vel (Fig. B6), comparison with giant and supergiant spectra suggests that KV Car may be a relatively massive and luminous AGB star

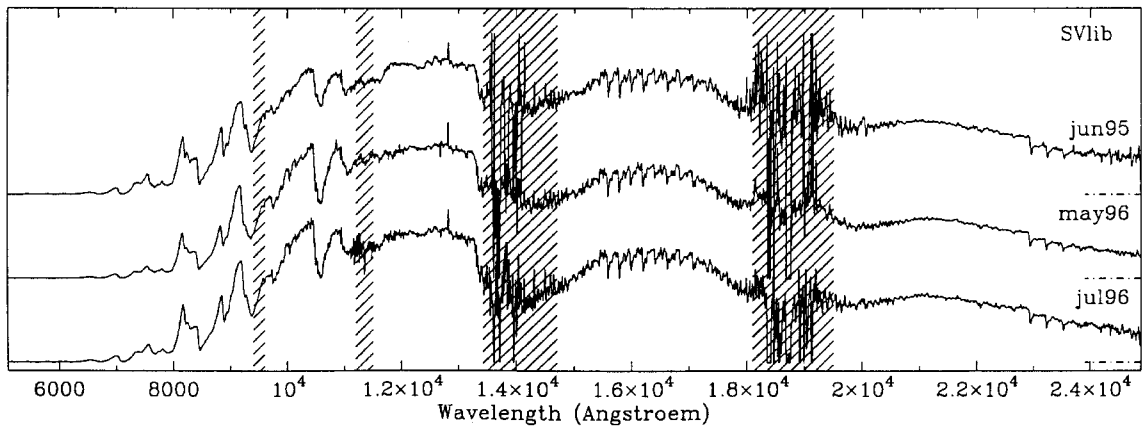


**Fig. B5.** SV Lib:  $P = 402.7$ ,  $\delta V = 1.3$  (see however Appendix A). Note the clean CO spectrum between  $1.55$  and  $1.7 \mu\text{m}$ , reminiscent of the S/C Mira BH Cru (Fig. B28). Phases: see Appendix A

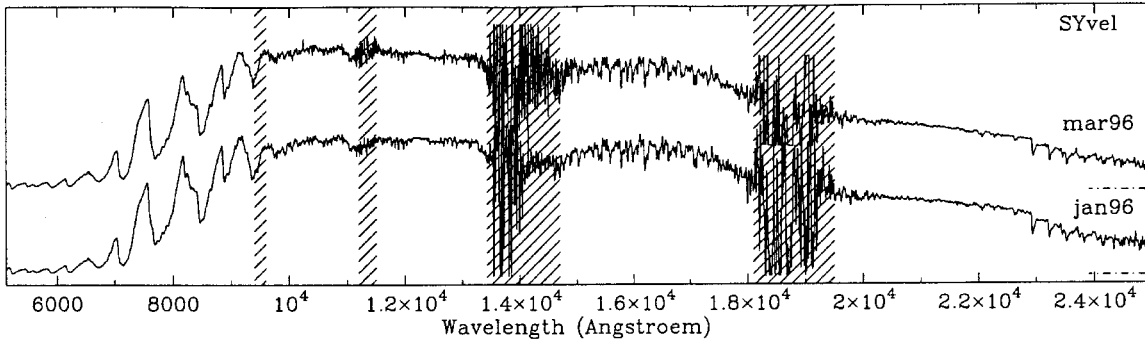


**Fig. B6.** SY Vel:  $P = 63.0$ ,  $\delta V = 1.3$ . Comparison with the giant BS 4267 (Fig. B1) and with the supergiant HD 115283 (Fig. B2) suggests this may be a relatively massive/luminous AGB star

### B.3. Other solar neighbourhood O-rich LPVs

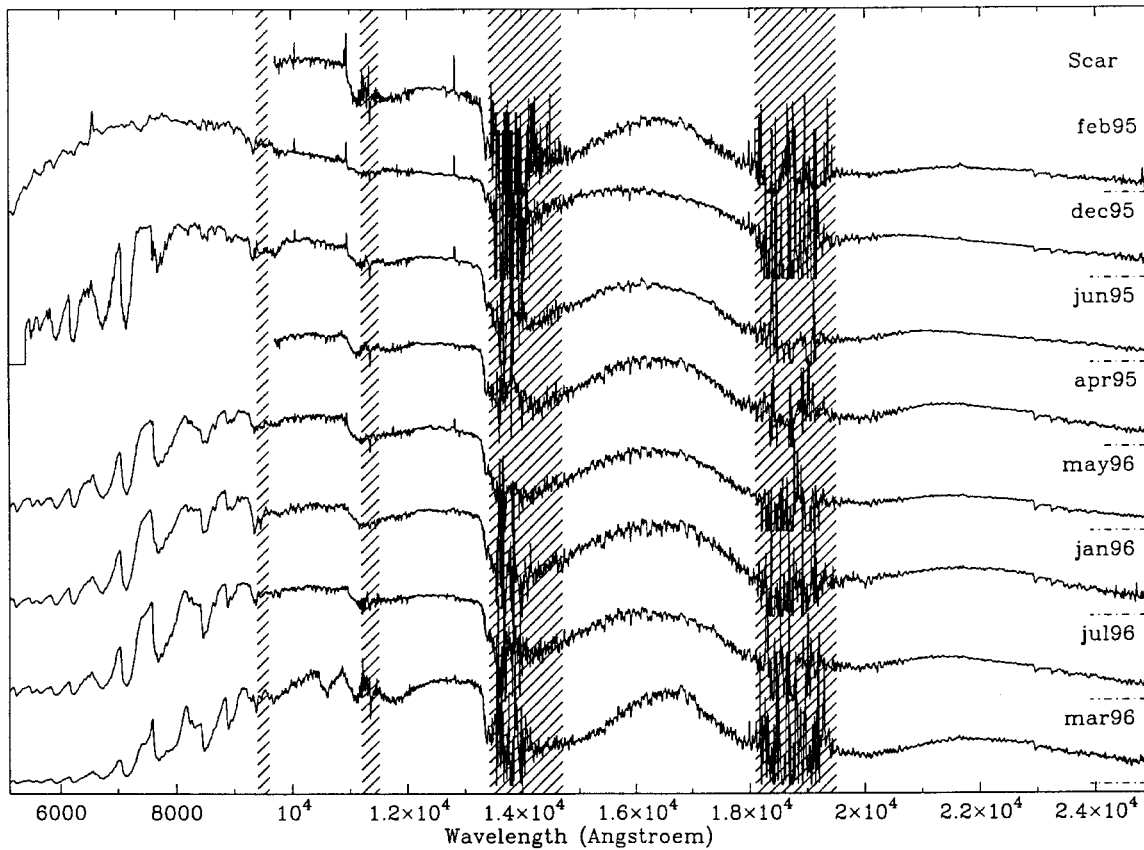


**Fig. B7.** S Car:  $P = 149.5$ ,  $\delta V = 5.4$ . Cycle to cycle variations are obvious: the three top spectra correspond to maximum light in successive cycles, the two bottom ones to minimum light. Approx. AAVSO/AFOEV phases from top to bottom: 0.1–0.0–0.9–0.4–0.2–0.4–0.5–0.6

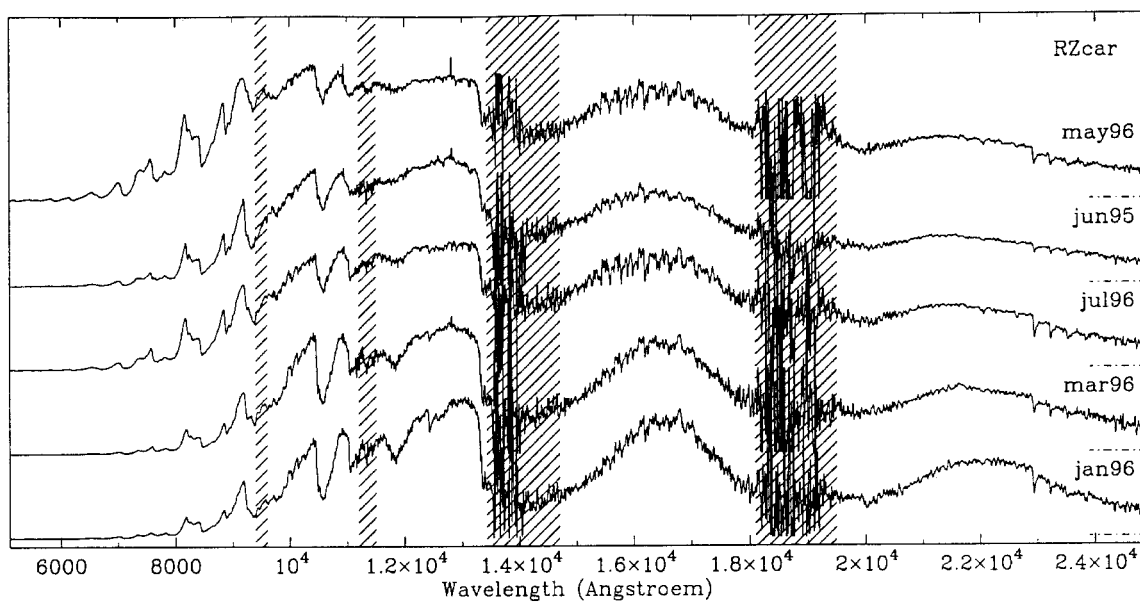


Fig. B8. RZ Car:  $P = 272.8$ ,  $\delta V = 6.2$ . GCVS phases from top to bottom: 0.0-0.8-0.2-0.7-0.6

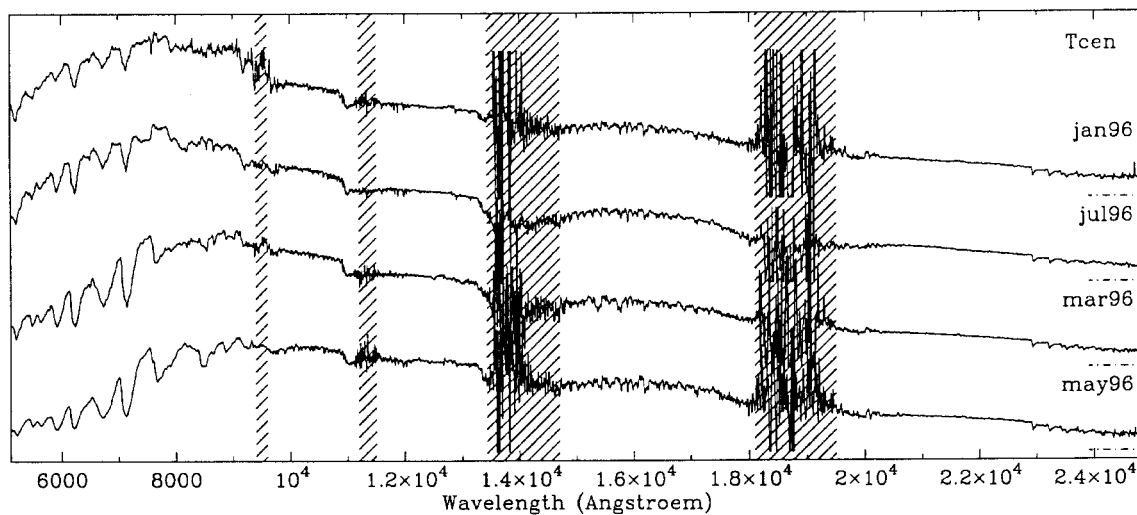


Fig. B9. T Cen:  $P = 90.4$ ,  $\delta V = 3.5$ . GCVS phases from top to bottom: 0.0-0.8-0.4-0.3

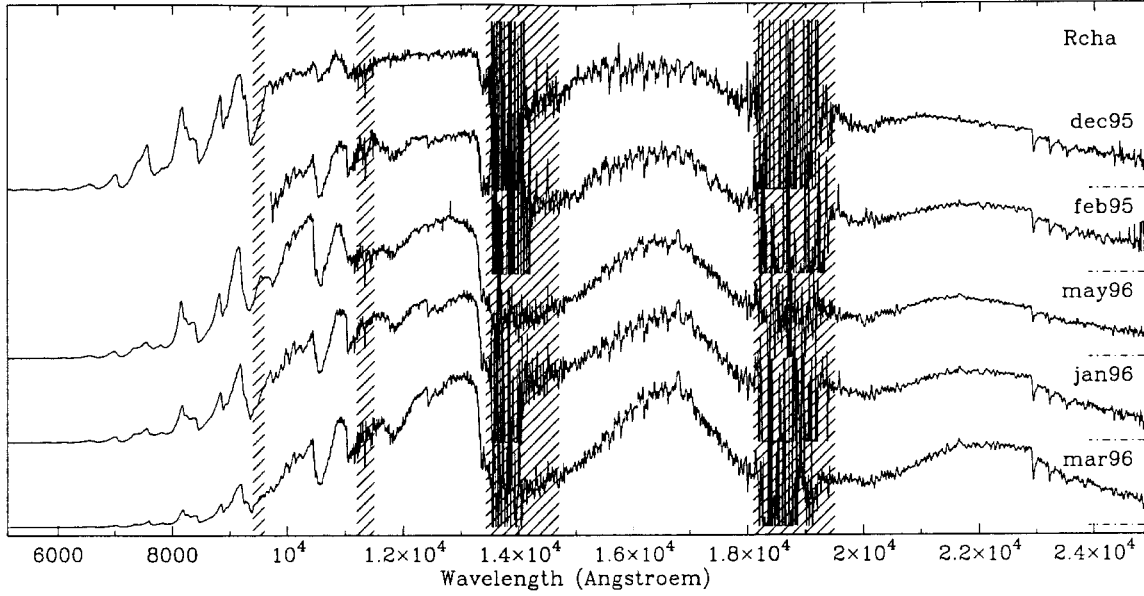


Fig. B10. R Cha:  $P = 334.6$ ,  $\delta V = 6.7$ . GCVS phases from top to bottom: 0.1–0.2–0.6–0.3–0.3 (doubtful values)

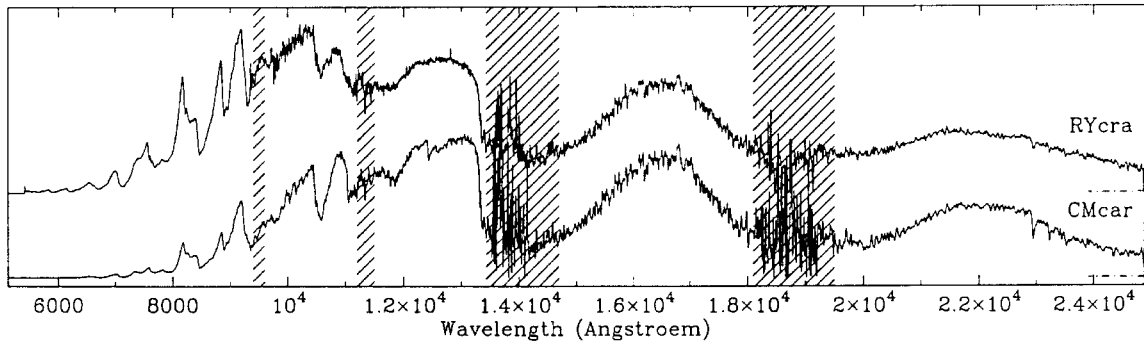


Fig. B11. RY Cra (Jun. 95, GCVS phase 0.9):  $P = 195$ ,  $\delta V = 1.9$ ; CM Car (Jan. 96, GCVS phase 0.4):  $P = 335$ ,  $\delta V = 2.5$ . CM Car resembles X Men at a phase close to 0.5, and RY Cra resembles X Men at maximum

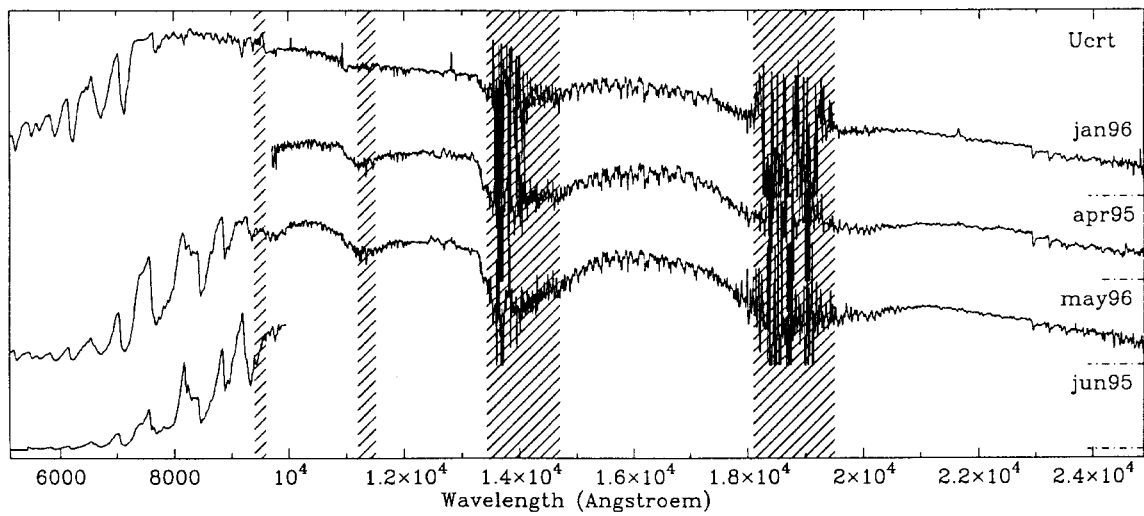


Fig. B12. U Crt:  $P = 169.0$ ,  $\delta V = 4$ . The single VI spectrum plotted to illustrate the cool temperatures reached by this star. The available data covers the range M1–M7 in spectral type (instead of staying close to M0 as given in the GCVS). GCVS phases from top to bottom: 0.2–0.5–0.9–0.8 (doubtful values; probably too high by about 0.3 cycles)

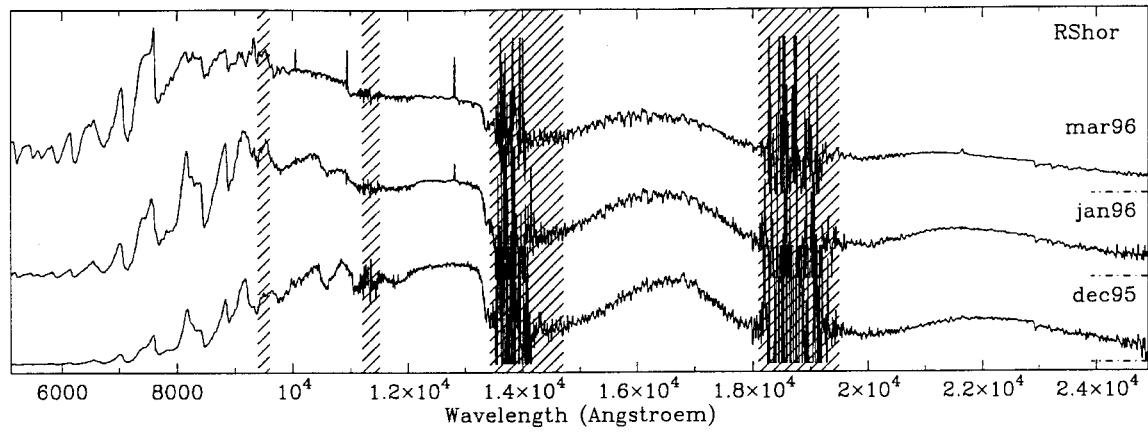


Fig. B13. RS Hor:  $P = 202.9$ ,  $\delta V = 5.2$ . GCVS phases from top to bottom: 0.8–0.6–0.4

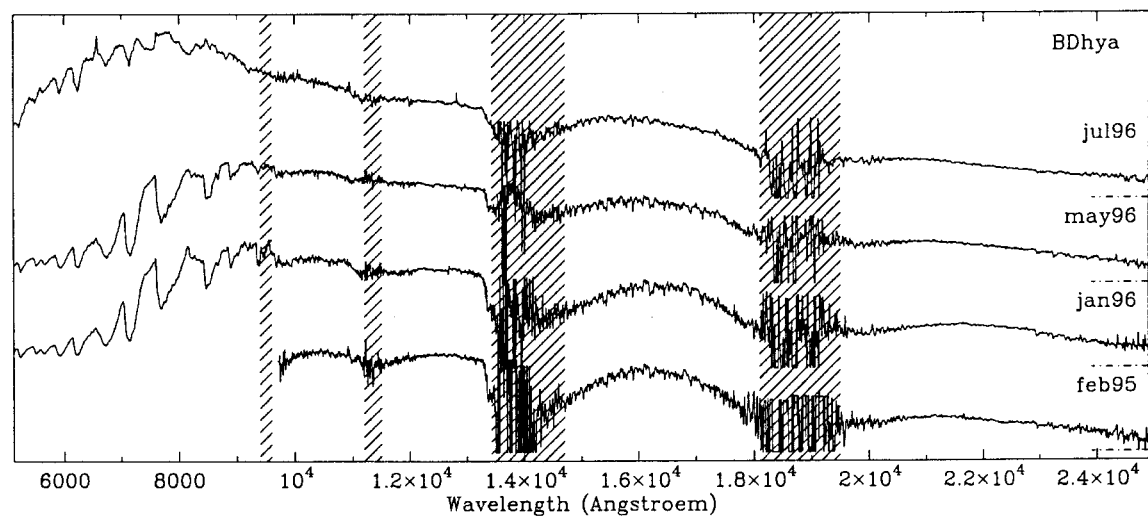
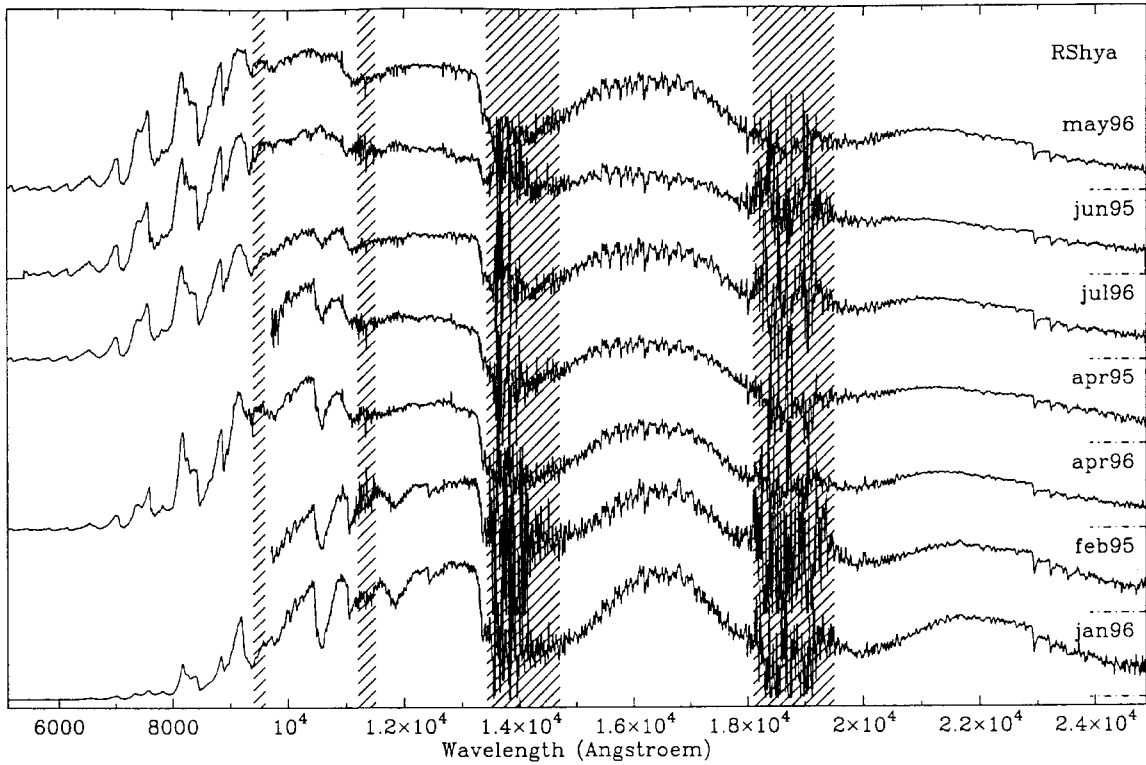
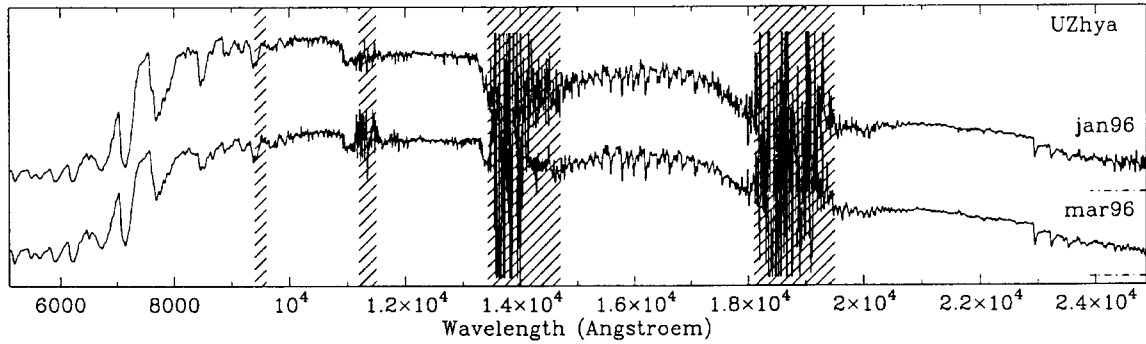


Fig. B14. BD Hya:  $P = 117.4$ ,  $\delta V = 1.8$ . GCVS phases from top to bottom: 0.6–0.2–0.2–0.2 (doubtful values, top spectrum probably closer to maximum)



**Fig. B15.** RS Hya:  $P = 338.6$ ,  $\delta V = 5.2$ . GCVS phases from top to bottom: 0.7-0.6-0.8-0.5-0.5-0.3-0.3 (doubtful values)



**Fig. B16.** UZ Hya:  $P = 261.0$ ,  $\delta V = 5.7$ . GCVS phases from top to bottom: 0.0-0.2

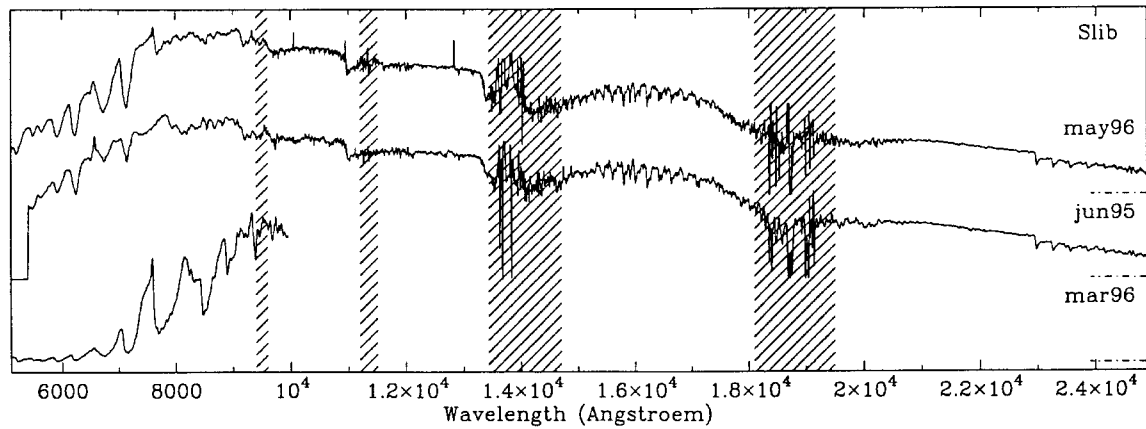


**Fig. B17.** S Lib:  $P = 192.9$ ,  $\delta V = 5.5$ . The unmatched VI spectrum is plotted to illustrate the cool temperatures reached by this star. The 15 days delay between the optical and NIR observations in June 95 may explain the absence of  $P\beta$  emission despite the strong  $H\alpha$  line. GCVS phases from top to bottom: 0.3-0.5-0.8 (doubtful values; probably too high by about 0.3 cycles)

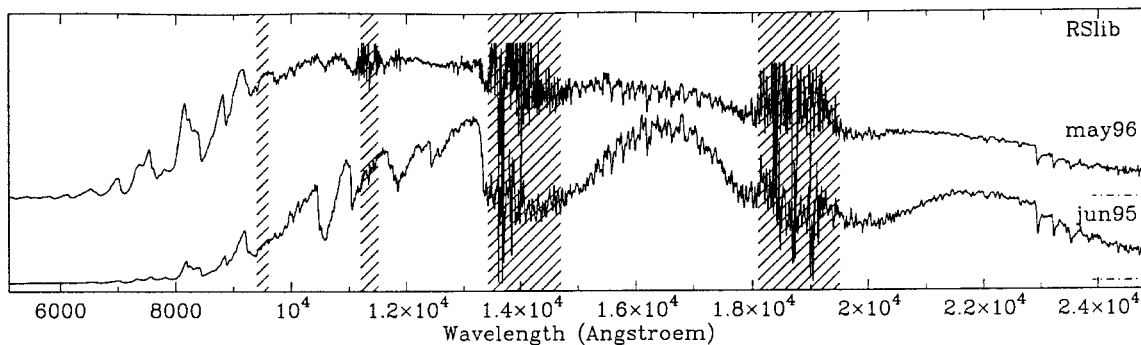


Fig. B18. RS Lib:  $P = 217.6$ ,  $\delta V = 6.0$ . GCVS phases from top to bottom: 0.1–0.5

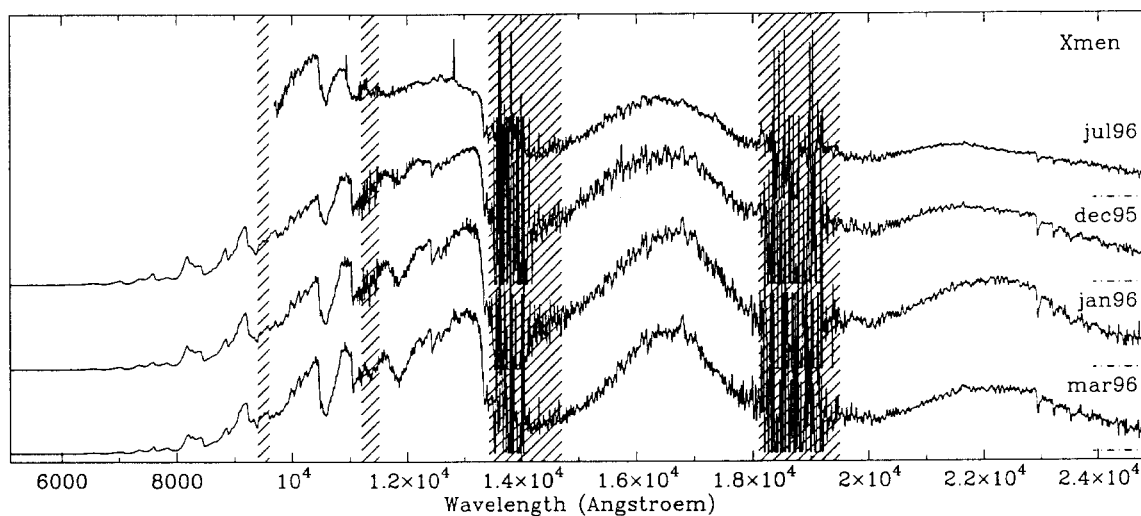


Fig. B19. X Men:  $P = 380.0$ ,  $\delta V = 3.6$ . GCVS phases from top to bottom: 0.7–0.2–0.3–0.4 (doubtful values; probably too low by about 0.2 cycles)

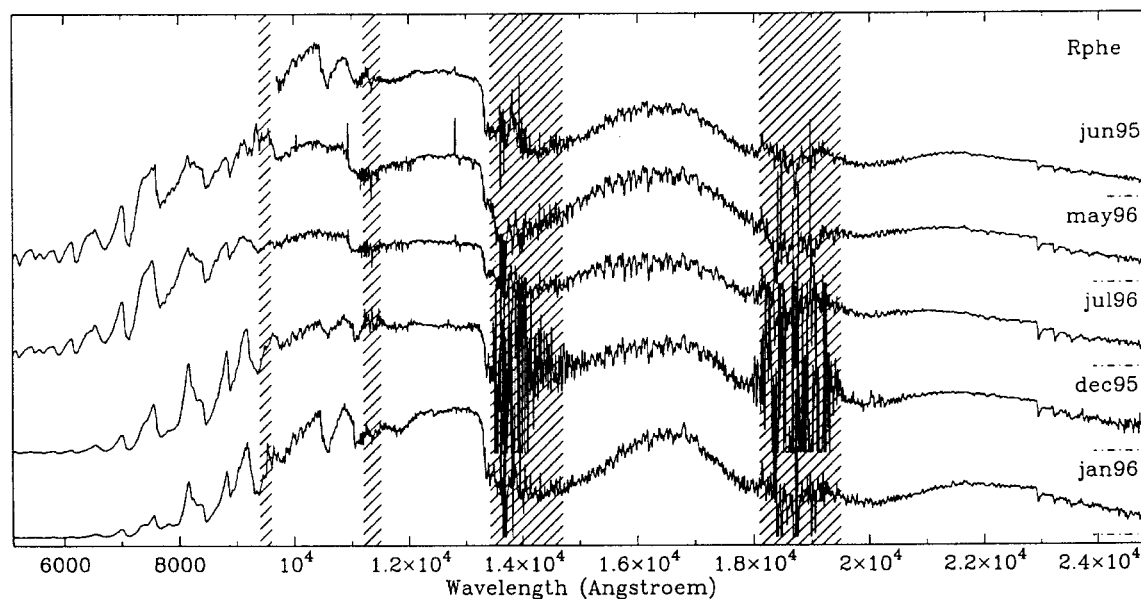


Fig. B20. R Phe:  $P = 269.3$ ,  $\delta V = 6.9$ . GCVS phases from top to bottom: 0.6–0.9–0.0–0.3–0.5 (in good agreement with AAVSO light curve)

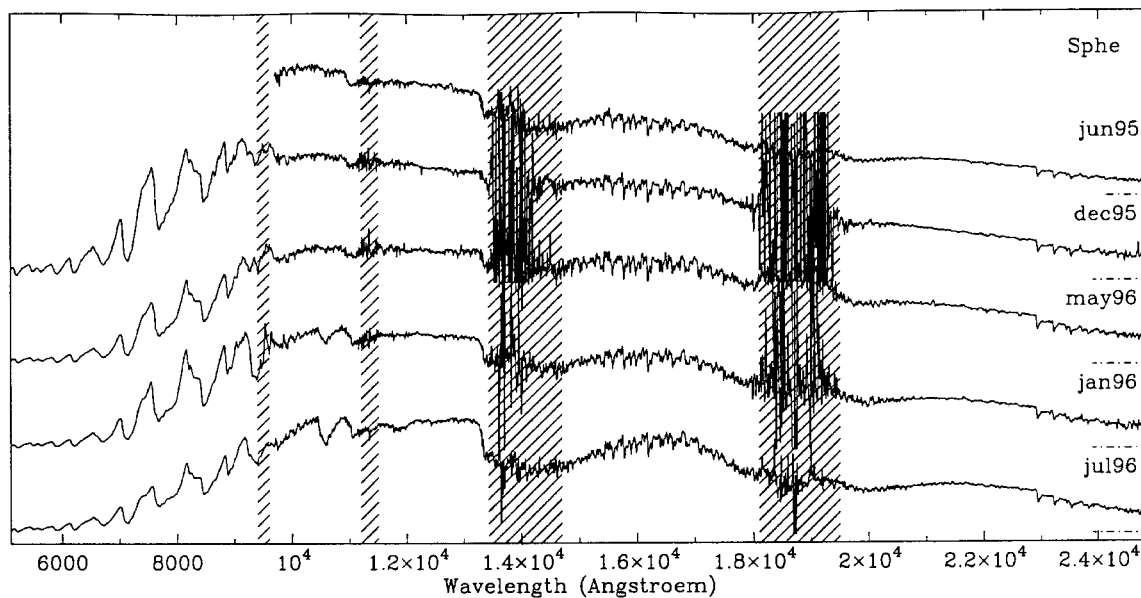


Fig. B21. S Phe:  $P = 141.0$ ,  $\delta V = 2.0$ . GCVS phases from top to bottom: 0.6–0.9–0.1–0.2–0.4 (doubtful values)

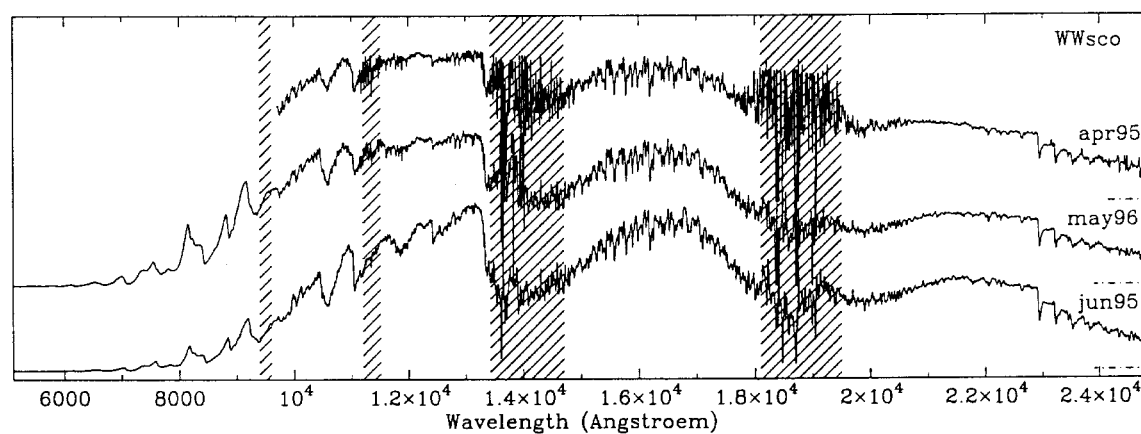


Fig. B22. WW Sco:  $P = 431$ ,  $\delta V = 4.1$ . Potentially metal rich star. GCVS phases from top to bottom: 0.3–0.3–0.5

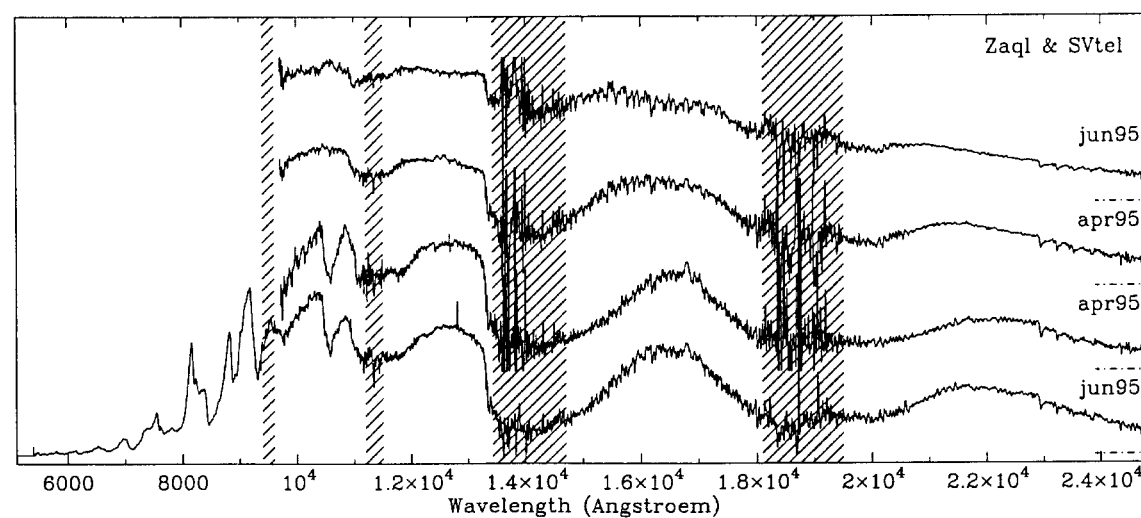
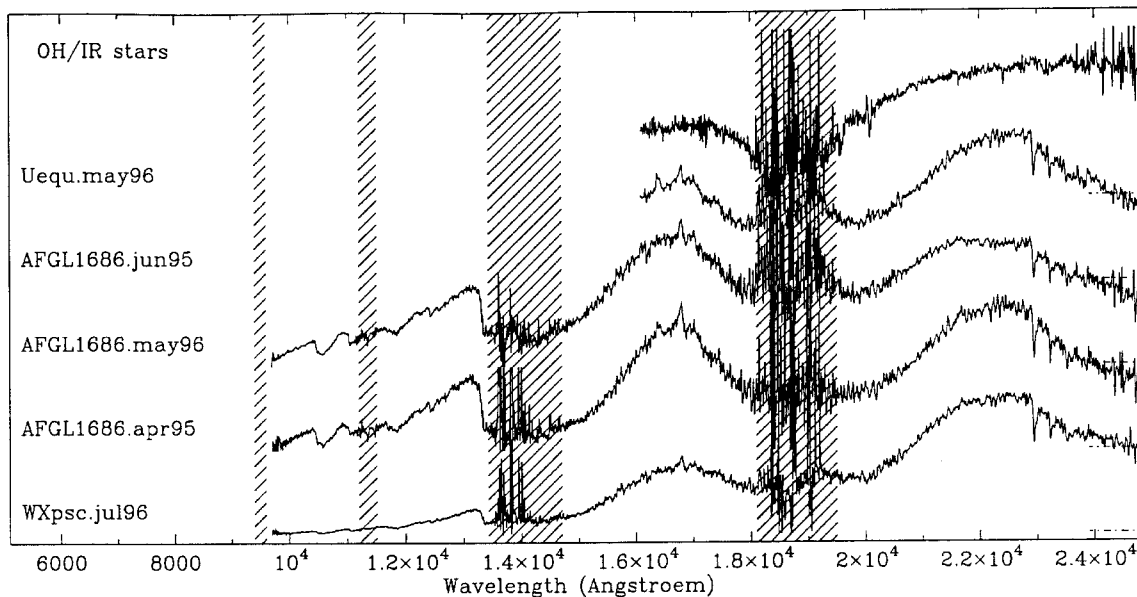


Fig. B23. Upper 2 spectra: Z Aql:  $P = 129.2$ ,  $\delta V = 6.6$ ; bottom 2 spectra; SV Tel:  $P = 225.5$ ,  $\delta V = 3$ . GCVS phases from top to bottom: 0.5–0.0 for Z Aql, 0.7–0.0 for SV Tel

#### B.4. Obscured O-rich LPVs



**Fig. B24.** OH/IR stars. The quasi-absence of CO absorption in U Equ indicates CO or circumstellar dust emission for this star, while circumstellar dust absorption is probably partly responsible for the red colours of the others

#### B.5. O-rich LPVs in the Galactic Bulge

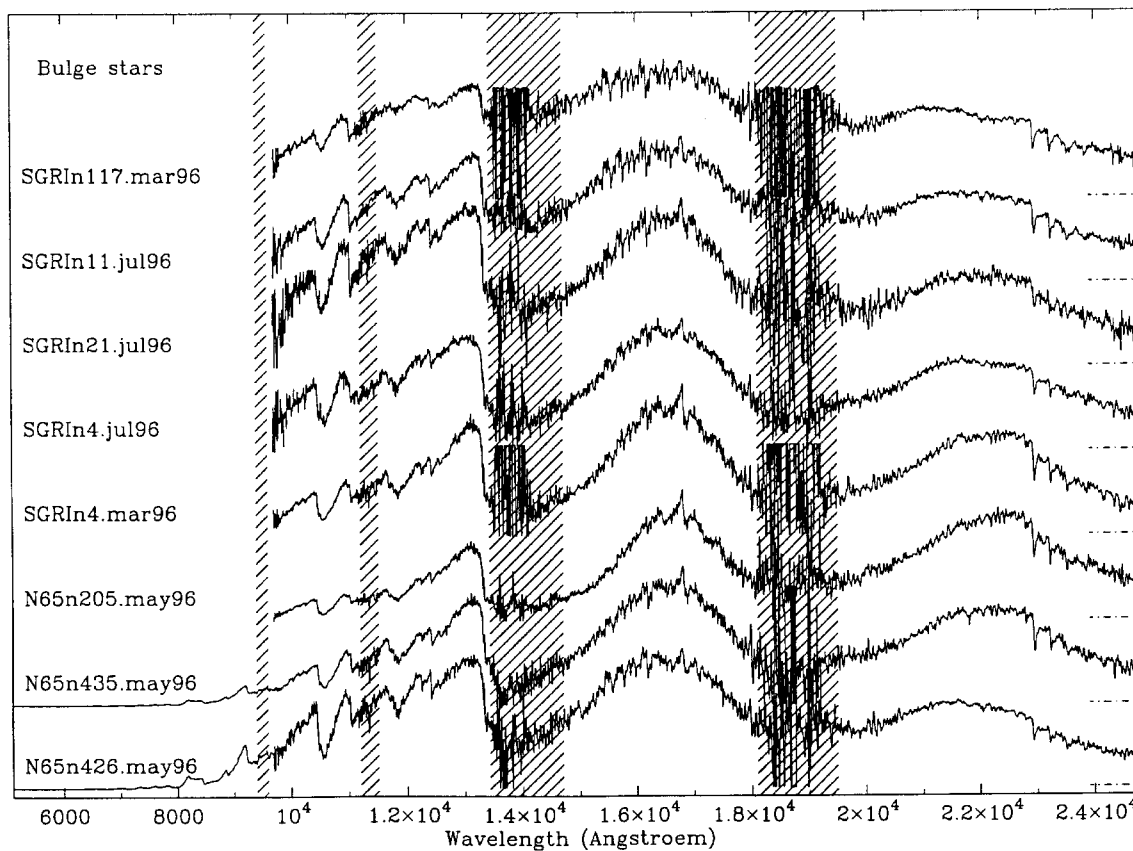


**Fig. B25.** Bulge LPVs

B.6. Luminous red O-rich stars in the LMC and SMC

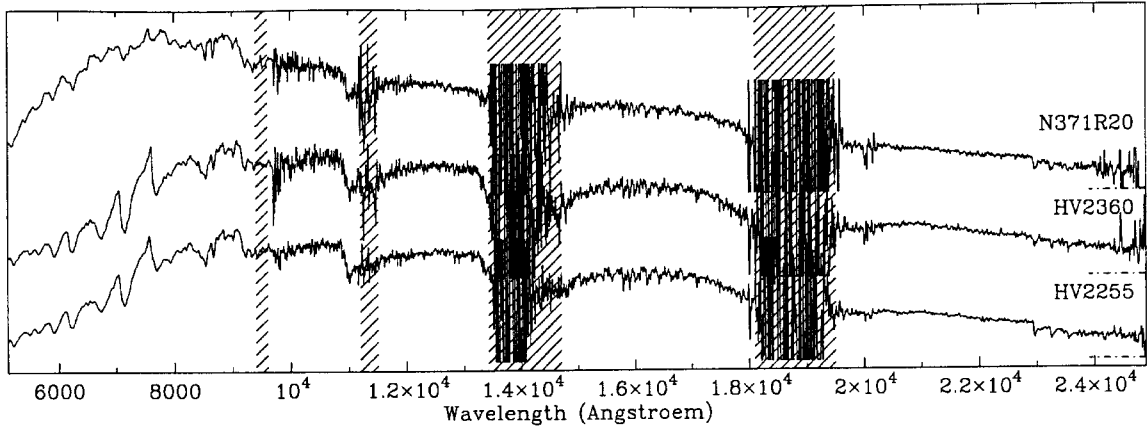


Fig. B26. Luminous red stars in the LMC (HV 2255 and HV 2360) and in the SMC (N371R20)

B.7. C-rich LPVs

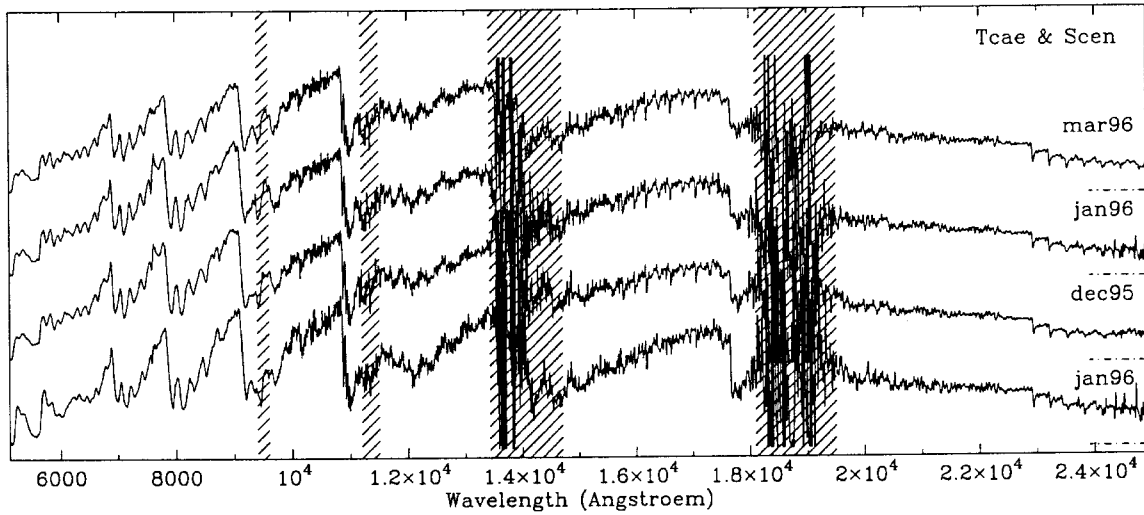


Fig. B27. Bottom spectrum: S Cen:  $P = 65$ ,  $\delta V = 1.5$ . Top 3 spectra: T Cae:  $P = 156$ ,  $\delta V = 1.8$ . Carbon stars. GCVS phases for T Cae from top to bottom: 0.0–0.8–0.4

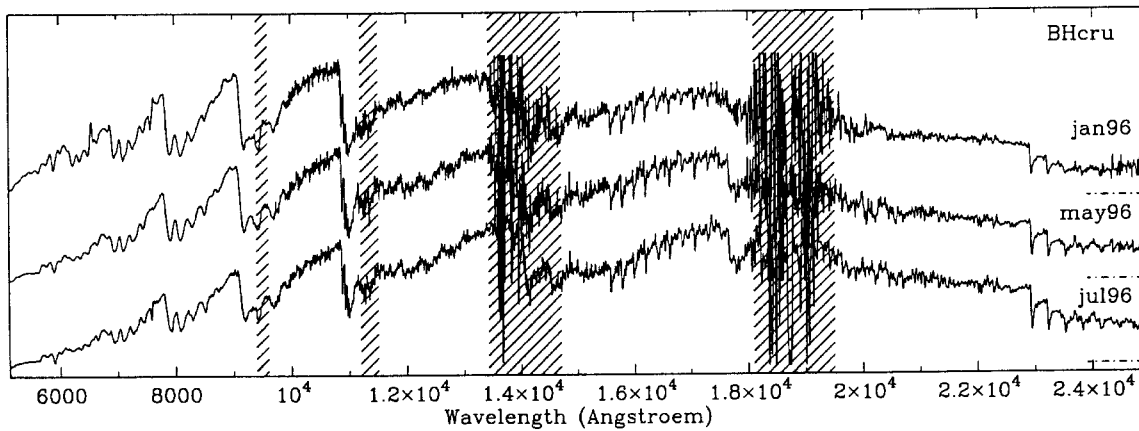


Fig. B28. BH Cru:  $P = 520$ ,  $\delta V = 2.8$ . S/C star whose period increased from 421 to about 535 days over the last 20 years (Bedding et al. 2000). The unmatched optical spectrum taken in March 1996 (not shown) also displays  $H\alpha$  emission. GCVS phases from top to bottom: 0.0–0.3–0.4 (in good agreement with AAVSO data)

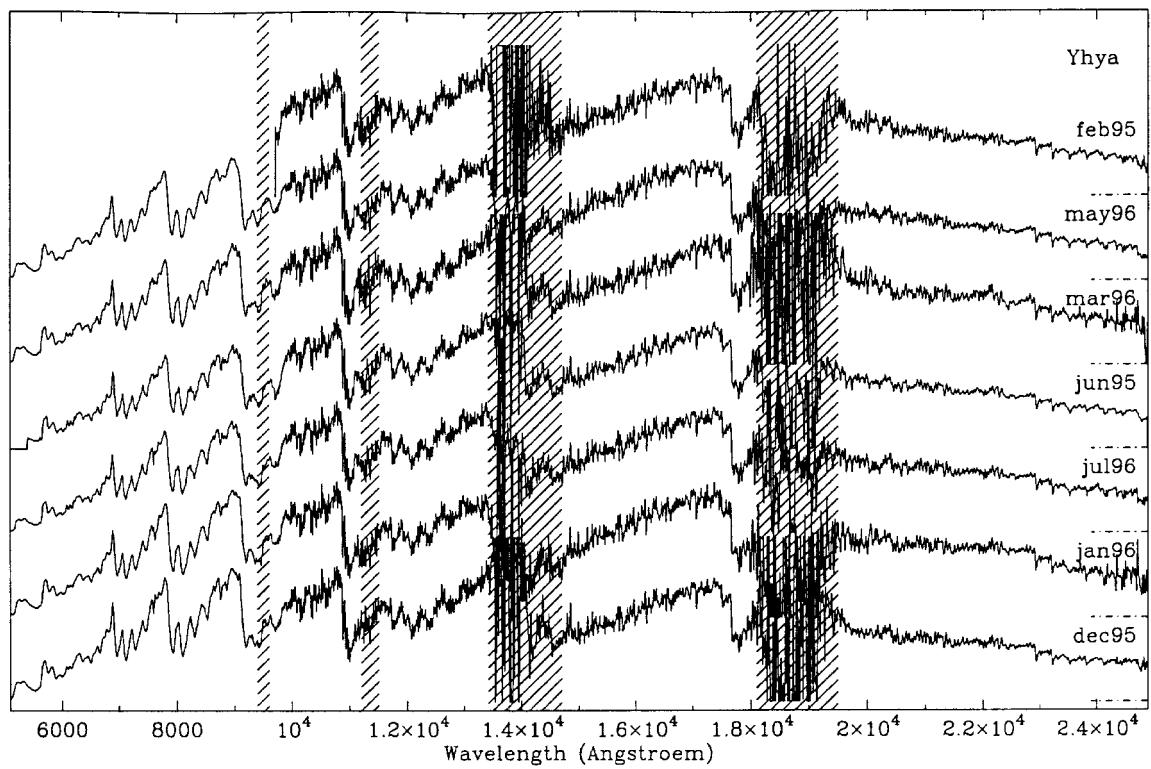


Fig. B29. Y Hya:  $P = 302.8$ ,  $\delta V = 3.7$ . Carbon star

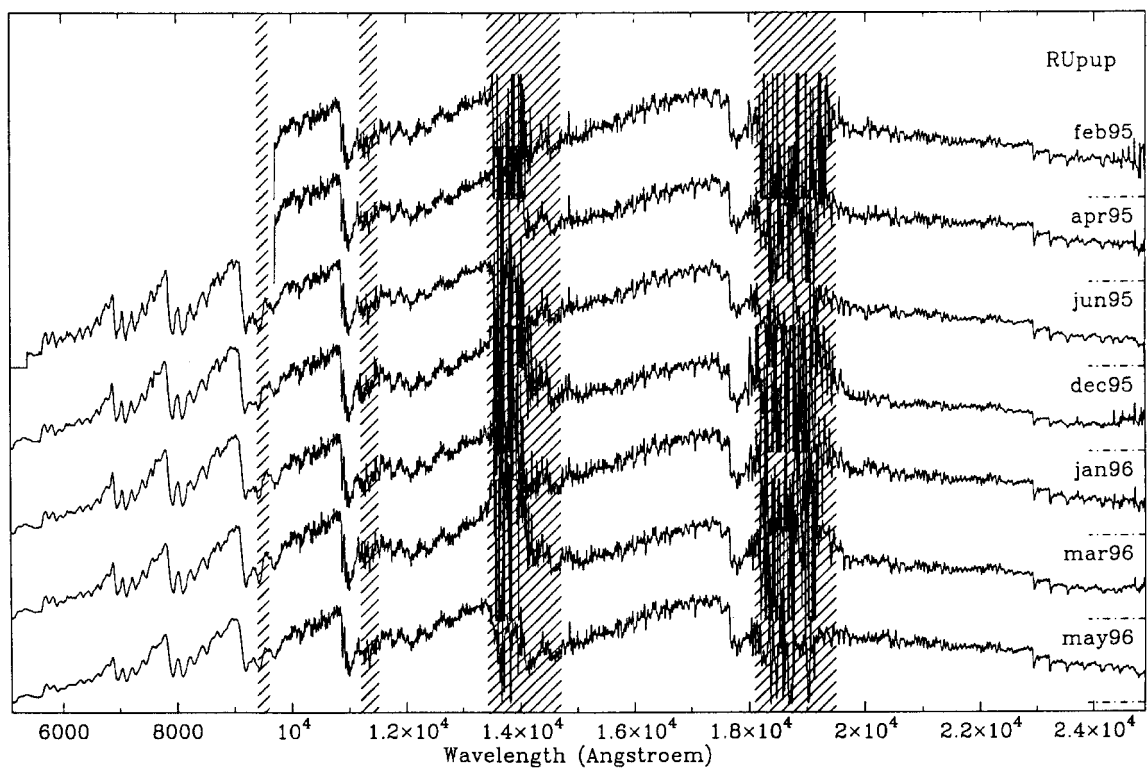
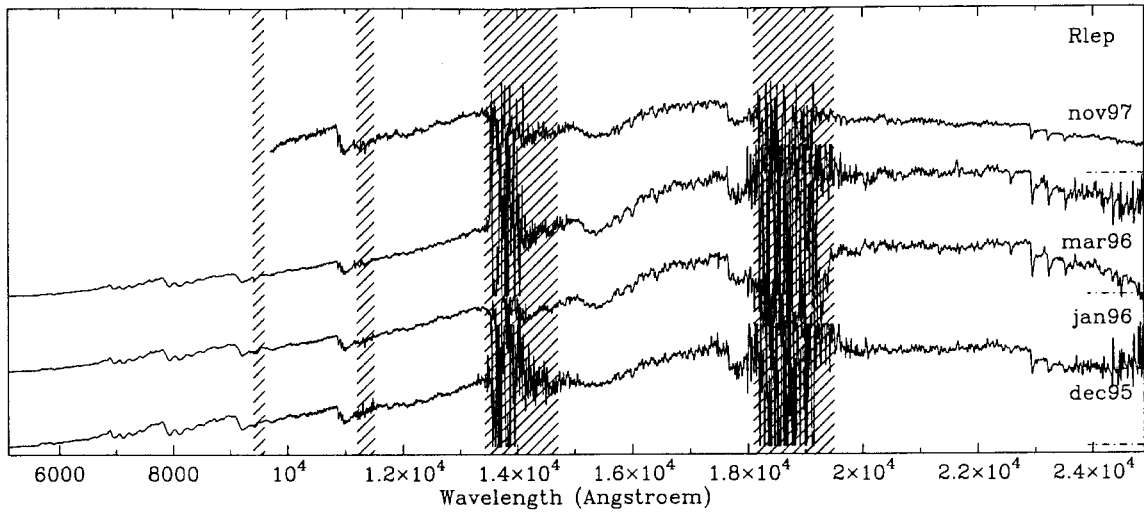


Fig. B30. RU Pup:  $P = 425$ ,  $\delta V = 1.9$ . Carbon star

*B.8. Obscured C-rich LPV*

**Fig. B31.** R Lep:  $P = 427.1$ ,  $\delta V = 6.2$ . Carbon star. GCVS phases from top to bottom: 0.3–0.9–0.8–0.7 (doubtful values, bottom 3 spectra probably closer to minimum, as also suggested by AFOEV data)